ORNL/SPR-2022/2631

Hierarchical Model-Free Transactive Control of Building Loads to Support Grid Services

Mohammed Olama
Kadir Amasyali
Yang Chen
Christopher Winstead
Byungkwon Park
Teja Kuruganti
Seddik Djouadi
Bhagyashri Telsang

October 2022

OAK RIDGE NATIONAL LABORATORY
MANAGED BY UT-BATTELLE FOR THE US DEPARTMENT OF ENERGY

ORNL/SPR-2022/2631

Computational Sciences and Engineering Division

HIERARCHICAL MODEL-FREE TRANSACTIVE CONTROL OF BUILDING LOADS TO SUPPORT GRID SERVICES

Mohammed Olama
Kadir Amasyali
Yang Chen
Christopher Winstead
Byungkwon Park
Teja Kuruganti
Seddik Djouadi
Bhagyashri Telsang

Date Submitted: 10/15/2022

Prepared by
OAK RIDGE NATIONAL LABORATORY
Oak Ridge, TN 37831-6283
managed by
UT-BATTELLE, LLC
for the
US DEPARTMENT OF ENERGY
under contract DE-AC05-00OR22725

CONTENTS

LIST OF FIGURES

LIST OF TABLES

ACKNOWLEDGMENT

This material is based upon work supported by the U.S. Department of Energy, Office of Energy Efficiency and Renewable Energy, Building Technologies Office under Award Number 34522.

EXECUTIVE SUMMARY

Residential buildings consume 4.4 quads of electricity annually, approximately 37% of the total electricity consumption in the United States. This represents a vast resource that can be used for demand management and other ancillary services. This project aims to develop a robust, scalable hierarchical transactional control mechanism incorporating elements of model-free control (MFC) and game theory to harness buildings to provide ancillary services to the grid. This approach is being taken to address the challenges of incorporating traditional transactional control schemes into existing buildings. The challenges include small individual building sizes requiring aggregation of many buildings, unpredictable energy usage that makes model identification difficult, and satisfying the sensitive occupant comfort constraints. In the proposed approach, by separating the control mechanism into two layers above and below the load aggregator, MFC can be used below the aggregator to modulate flexible building loads in response to pricing signals with guaranteed performance. This allows the burden of identifying an accurate model of the system to be shifted to the above-aggregator layer, where fluctuations in individual building usage have less impact on predicted building system behavior. Game theory concepts can then be used to determine pricing curves and control signals among regional aggregators. Managing this control in a game-theoretic approach will allow us to build in financial incentives that increase customer engagement. Additionally, the usage of MFC necessitates less burdensome computational and communication requirements, thus, it is easily deployable on small, embedded devices.

In a broader sense, developing a strategy capable of effectively incorporating residential and small commercial buildings will allow greater throughput of existing and emerging grid services in addition to future transactive energy grid management methods. Using MFC within a hierarchical control architecture will allow the shifting of existing forecasting challenges to an aggregate level, where dynamics are slower and more predictable. This will enable a smooth interface between the grid services requests of utilities and the reliable control required by participating buildings. MFC, which supports distributed control architecture, permits a scalable solution that can be deployed to neighborhood-size systems as well as individual buildings.

This project focuses on three objectives: (1) developing the mathematical framework, algorithm toolkit, and software toolset of the two-layer transactive control testbed; (2) developing a scalable solution for application over many residential and small-size commercial buildings with sparse distributed communication; and (3) field testing and implementation on hardware of the control strategies developed in the previous two objectives. The research and development activities are focused and designed to be impactful within the relevant 2025 targets timeframe. An open-source control framework for exploiting variability and dispatchability of building loads will be delivered as the outcome of the project. This capability enables greater participation of loads in electricity markets and ancillary services that are both useful for the utility and financially beneficial for building owners.

1. BACKGROUND

Due to the increasing concerns over climate change, the penetration of renewables has been increasing all over the world. For example, in the United States, the share of electricity generation from renewables has increased from 9% to 17% over the past 10 years and is expected to increase to 42% by 2050 [1]. Traditionally, the balance between the electricity supply and demand has been sustained through demand-driven control techniques in which electricity generation is adjusted in response to the changes in the demand. Demand-driven control techniques are effective for power systems where the supply-side is dependent on fossil fuels. In such power systems, electricity generation can easily be ramped up or down in response to an instantaneous electricity demand due to the ample ramping capabilities of fossil fuels. Yet, demand-driven control techniques are not applicable for modern power systems with high renewable penetration. Unlike fossil fuels, renewables do not have sufficient ramping capabilities due to their variable, intermittent, and unpredictable nature. For this reason, modern power systems utilize supply-driven control techniques that aim to control electricity demand in response to the changes in the supply [2]. Consequently, modern power systems require flexible demand-side resources to maintain the balance between electricity supply and demand [3].

Buildings, as major electricity consumers, are one of the greatest demand flexibility assets [4]. Thermostatically controlled loads (TCLs) in buildings, such as heating, ventilation, and air conditioning (HVAC) units and water heaters (WHs), account for a significant portion of buildings' electricity consumption. Because TCLs are operated within a comfort temperature range to swing inside, they provide the ability to store thermal energy. With a proper coordination, building TCLs can be manipulated to draw electricity demand at desirable levels when needed while still maintaining the comfort of end users. Thus, the coordinated aggregation of building TCLs can be excellent demand-side management resources [5, 6]. In this regard, demand response (DR) programs have long been used by grid operators to enable the coordination of a large number of grid-interactive efficient buildings (GEBs) [7]. In addition, many home and building energy management systems have been developed to facilitate the integration of GEBs to DR programs [8].

An electricity market includes various stakeholders such as distribution system operators (DSOs), load aggregators (LAs), and end users [9]. Therefore, it is essential to determine effective transactive control structures that can accommodate the interests of all stakeholders. In this regard, a two-level market structure in which the two levels are connected by the LAs is often utilized. In this structure, the role of LAs is crucial because they are employed as central agents that execute DR programs and interact with the DSO on behalf of the end users [10]. Specifically, the LAs negotiate the day-ahead electricity price with the DSO for the aggregated load of the end users, which results in an optimal pair of price and aggregated load. The role of the LAs is critical because they also need to control the loads of the end users in a way that maintains the quality of service provided to their end users while following the reference aggregated load power profiles resulted in the negotiations with the DSO.

In a DR program, an operator, the DSO, purchases the electricity from different resources available in the wholesale market at a cost and sells the purchased electricity to end users at a price. When determining the price, the DSO will have several objectives such as increasing its profit and enhancing the reliability of the grid. The end users, on the other hand, adjust their electricity consumption in a way that minimizes their electricity cost while maintaining their comfort. In recent years, there has been a significant research attention in demand flexibility, and the effectiveness of DR in many areas has been proven. In this regard, many review studies on DR have been conducted to classify and compare existing methods. For example, [11] provided a comprehensive review on demand-side management (DSM). In [12], the authors conducted an exhaustive review on residential DSM architectures, approaches, optimization models, and methods. Accordingly, the DR programs can be classified based on either their ways to engage end users or control strategies.

In terms of ways to engage end users, DR programs can broadly be categorized as price-based, direct-load control, and transactive control methods [13-15]. Price-based DR programs use dynamic price signals to incentivize or disincentivize consumption patterns of end users. However, these programs do not engage the end users in the pricing process and require an accurate modeling of end-user reactions in response to given electricity prices, and failure to do so can ultimately result in poor grid stability. Direct-load control programs enable DR operators to remotely control specific end-user loads. Such programs do not require any modelling efforts because the changes in electricity consumption is certain as it is directly controlled by the DR operator. However, these programs may violate the preferences and privacy of end users. Transactive control programs use market mechanisms to attract end users to provide DR. Such programs engage the end users in the pricing process using a set of optimization (negotiation) mechanisms that comply with their preferences. The most commonly used optimization mechanisms are the game theoretical mechanisms [16-19], metaheuristic mechanisms [20, 21], and parameterization-based mechanisms [22]. The main challenge associated with transactive control is to coordinate and aggregate the loads of end users. For a successful DR program, an effective and efficient coordination and control of a very large number of geographically distributed GEB is essential.

In terms of control strategies, DR programs can broadly be categorized as rule-based, model-based, and reinforcement learning (RL)-based methods [23, 24]. Rule-based controllers (e.g., [25]) are one of the most popular control approaches used in DR due to their simplicity. These approaches simply rely on a set of simple heuristics that are derived based on expert knowledge. For this reason, the success of rule-based controllers mainly depends on the expertise and knowledge of the users. However, these approaches may not be suitable for dealing with complex, multiple, and/or nonlinear objectives. Model-based controllers are planning-based approaches that optimize a control problem over receding time. These controllers require accurate models that define the system dynamics. However, obtaining such models requires a significant amount of time and effort. On the contrary, RL-based approaches are potentially model free and can help alleviate the limitations associated with model-based approaches. Nevertheless, these approaches learn an optimal control policy by interacting with the surrounding environment and thus may take a long time to learn [26].

In terms of solution approaches, bilevel optimization has been widely used for developing market-based control approaches due to its ability to capture the interaction between the strategic decision making of the different parties involved in DR [27]. Bilevel optimization problems are usually solved using centralized approaches such as the backward induction (BI) method (e.g., [28-30]), in which a central unit collects all the necessary information and plans accordingly. Centralized approaches are, however, computationally expensive and may arise privacy concerns among the participants of DR [31]. Also, centralized approaches are not fault tolerant. For instance, an issue affecting the DSO may cause the failure of the entire system [32]. For this reason, distributed approaches have attracted widespread research interests in recent years (e.g., [33]). In distributed approaches, the LAs are responsible for making their own decisions based on the information provided by the DSO.

LAs can control both building non-TCLs (e.g., washers and dryers) and building TCLs (e.g., HVACs and water heaters). Existing studies have utilized several ways to maintain the quality of service that the LAs provide to the end users. For building non-TCLs, the LAs aim to follow the schedule of the end users as much as possible. As such, certain time constraints that are determined by the end-users are often used to guarantee the quality of service (e.g., [34]). For building TCLs, the LAs aim to maintain the thermal comfort of the end users. There are various control approaches to maintain thermal comfort. For example, the works in [6, 9, 35-37] used model-based control approaches (e.g., resistance-capacitance (RC) models, reduced-order models) to simulate TCLs and compute the resulting temperatures. Model-based control approaches, however, require the physical parameters of the building TCLs to accurately reflect their system dynamics. Considering that DR programs have a large number of participants, gathering all the physical parameters and developing an accurate model for each building TCL is impractical. To this end, recent studies (e.g., [38, 39]) have employed virtual batteries to compute the aggregated flexibility

that the TCLs can provide without sacrificing the comfort of the end users. Although virtual-battery-based control and coordination approaches do not require the modelling of each TCL, the physical parameters of the TCLs are still needed to develop a virtual battery model. Finally, some studies (e.g., [40-42]) used utility functions to quantify the level of satisfaction with thermal comfort. Despite their simplicity, such functions are very generic and often do not guarantee the actual satisfaction of end users.

Towards addressing the aforementioned limitations related to the ways to engage end users and control strategies, this project proposes a scalable hierarchical model-free transactional control approach that incorporates elements of virtual battery, game theory, and model-free control (MFC) mechanisms. The proposed approach separates control into upper and lower levels connected by LAs. The upper level is based on virtual battery and game theory. A one-leader (DSO) and multiple-follower (LAs) Stackelberg game is formulated to coordinate the aggregated GEB using day-ahead load scheduling and pricing. In addition, the concept of virtual battery is integrated into the game as a set of constraints for guaranteed thermal comfort of end users. The lower level is based on MFC, which is a novel online control strategy that does not require any modelling or training efforts and can be applied to both linear and nonlinear systems [43]. To the date, it has already been successfully implemented in many other domains [44, 45]. This project also proposes a data-driven, distributed hierarchical transactional control approach, where the machine learning is utilized to predict the temperature responses in a data-driven manner, which facilitates maintaining the thermal comfort of the end users. This approach can be used for many DR applications to provide benefits for both the DSO and LAs in the electricity market. Using this approach, the DSO maximizes its profit and minimizes the total demand peak-to-average ratio (PAR) of the system, whereas the LAs minimize their electricity cost while maintaining the quality of service provided.

This project contributes to the body of knowledge on three main aspects. First, this project couples the MFC with the game-theoretic control and proposes a scalable model-free transactive control approach. MFC does not require any modeling effort or model training for the various building loads. This is very beneficial since deriving an accurate model for every single unit participating in DR programs and obtaining all the parameters about the units (e.g., thermal coefficients, standby losses) are infeasible. Also, MFC is computationally efficient, easily deployable even on small, embedded devices, and can be implemented in real time. Second, this project integrates the concept of virtual battery into DR via the Stackelberg game. The concept of virtual battery enables efficient coordination and aggregation of a large number of flexible GEB with guaranteed thermal comfort of end users. Third, this project proposes a machine learning model to predict the hourly temperatures of TCLs for given day-ahead outdoor temperature and aggregated load profiles. The proposed model is purely data-driven and does not require any physical parameters of the various building TCLs.

2. THE DETERMINISTIC HIERARCHICAL MODEL-FREE TRANSACTIONAL CONTROL APPROACH

2.1 OVERVIEW

The proposed approach utilizes a two-level control architecture (see Figure 1). The architecture includes three parties: the DSO, LAs, and end users. The upper level is handled by a Stackelberg game and a set of virtual batteries. The Stackelberg game conducts the negotiation between the DSO and the LAs within the limits of the aggregate flexibility offered by the participating GEB. The virtual batteries assist with quantifying the aggregate flexibility that each LA can offer for a guaranteed thermal comfort of end users. The lower level has two objectives: (1) allocating a sufficient amount of power to all end users to ensure the comfort of end users are maintained, and (2) tracking the aggregated load profile determined in the upper level. Subsequently, the proposed hierarchical model-free transactional control approach includes three primary steps: determining the virtual battery constraints, computing the optimal power and price signals using a Stackelberg game, and allocating the optimal power to the loads of end users using MFC. In the next subsections, the concepts of virtual battery, Stackelberg game, and MFC are explained.

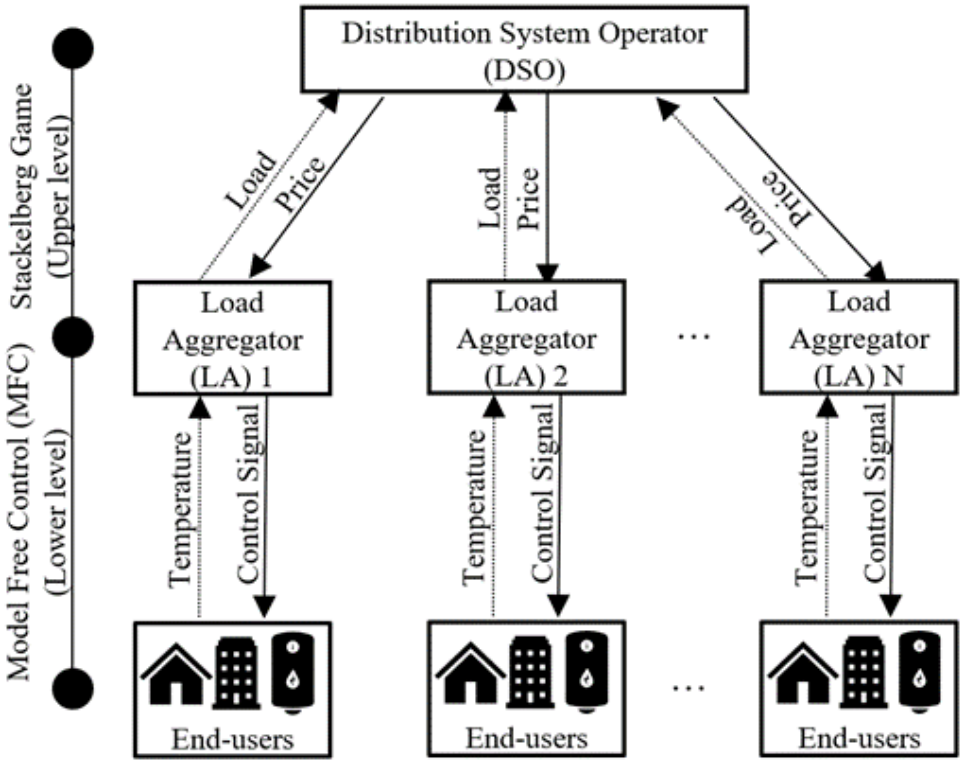

Figure 1. Overview of the proposed hierarchical model-free transactional control approach.

2.2 QUANTIFYING LOAD FLEXIBILITY USING THE VIRTUAL BATTERY MODEL

The virtual battery model assists in modelling the flexibility offered by a set of TCLs, including HVAC and WH units. For example, for a cooling scenario and assuming all TCLs have the same temperature setpoint (T_r) and comfort band (Δ), a fully charged battery means that the temperatures of the TCLs are $T_r - \Delta$. On the other hand, an empty battery means that the temperatures of the TCLs are $T_r + \Delta$.

The virtual battery model, adapted from [46, 47], determines whether a given power profile is feasible for a given set of TCLs. The feasibility of a power profile is defined by two criteria: (1) whether it can satisfy the comfort requirements of all TCLs, and (2) whether it can be tracked by the aggregate power consumption of all TCLs.

As mentioned earlier, the proposed approach is fully model free, and therefore it does not require the mathematical models of any building TCLs. The mathematical models presented in the remaining of this section are only used for simulating the considered TCLs (HVAC and WH units). In practice, only the periodical input-output measurements of the TCL units (i.e., input powers and output indoor/water temperatures) that are participating in the DR program are needed for the controller.

To simulate the residential and commercial HVAC units, the building thermal model depicted in Figure 2, adapted from [48], is used.

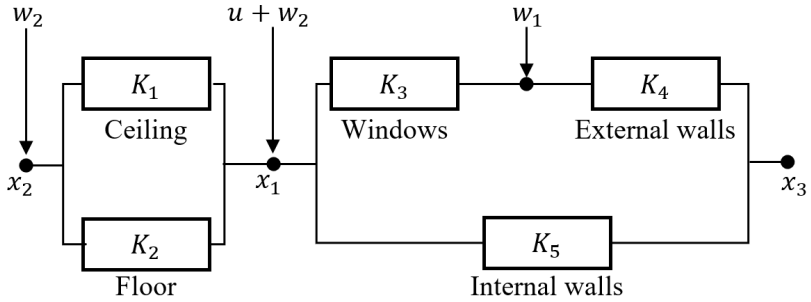

Figure 2. Schematic of the building thermal model.

The continuous-time dynamics of the building model are as follows:

$$\dot{x} = Ax + Bu + Gw \tag{1}$$

$$x = [x_1 \quad x_2 \quad x_3]^T, w = [w_1 \quad w_2]^T$$

$$y = Cx + Du \tag{2}$$

where x is the system state vector (x_1: room air temperature, x_2: interior-wall surface temperature, and x_3: exterior-wall core temperature), u is the on-off state of the HVAC, w is the vector of external disturbances (w_1: outdoor temperature, w_2 solar irradiance), and y is the system output (room air temperature). The system parameters A, B, C, D, and G are defined as follows:

$$A = \begin{bmatrix} \frac{-(K_1+K_2+K_3+K_5)}{C_1} & \frac{K_1+K_2}{C_1} & \frac{K_5}{C_1} \\ \frac{K_1+K_2}{C_2} & \frac{-(K_1+K_2)}{C_2} & 0 \\ \frac{K_5}{C_3} & 0 & \frac{-(K_4+K_5)}{C_3} \end{bmatrix},$$

$$B = \begin{bmatrix} \frac{COP_1 \times P_{m_1}}{C_1} \\ 0 \\ 0 \end{bmatrix}, C = \begin{bmatrix} 1 \\ 0 \\ 0 \end{bmatrix}', D = [0], G = \begin{bmatrix} \frac{K_3}{C_1} & \frac{\gamma}{C_1} \\ 0 & \frac{\gamma}{C_2} \\ \frac{K_4}{C_3} & 0 \end{bmatrix} \tag{3}$$

where K_1, K_2, K_3, K_4, and K_5 are the thermal conductivity values of ceiling, floor, windows, external walls, and internal walls, respectively; C_1, C_2, and C_3 are the heat capacity values of the air, interior wall, and exterior wall, respectively; P_{m_1}, COP_1, and γ are the rated power of the HVAC, coefficient of performance of the HVAC, and solar heat gain coefficient, respectively.

To simulate the WH units, the following model adapted from [49] is used:

$$\frac{\Delta T_w}{\Delta t} = \frac{\dot{Q} - UA \times (T_w - T_{amb}) - \dot{m} \times c_p \times (T_w - T_{fresh})}{c_p \times m} \tag{4}$$

$$\dot{Q} = \frac{P_{m_2} \times COP_2 \times \Delta t}{60}$$

where ΔT is the temperature change for a given time period Δt, $\dot{Q}$ is the heat added to the water tank, UA is the standby heat loss coefficient, T_w is the water temperature, T_{amb} is the ambient temperature, $\dot{m}$ is the mass flow rate, c_p is the specific heat of the water, T_{fresh} is the inlet water temperature, m is the mass of water, P_{m_2} and COP_2 are the rated power and coefficient of performance of the WH, respectively.

The aggregate nominal power for a set of GEB is defined as the power profile that is required to keep the TCLs in the set of GEB at their setpoints and maintain the operation of non-TCLs, such as pool pumps, washers, and dryers, in the set of GEB as desired by the occupants. There exist many data-driven methods (e.g., [50]) that predict the aggregate nominal power using weather forecasts and historical power usage data. In this pproject, the aggregate nominal power for a set of TCLs is determined by simply adding up the nominal power profiles for all HVACs and WHs. The nominal power for a single HVAC and a single WH can be computed by setting (1) and (4) to zero and extracting u and $\dot{Q}$, respectively. Consequently, the aggregate nominal power for a set of TCLs can be computed by

$$P_0 = \sum_{i=1}^{N} p_{0_i} \tag{5}$$

where P_0 is the aggregated nominal power for N heterogenous HVAC and WH units, and p_{0_i} is the nominal power for TCL i (HVAC or WH). On the other hand, the aggregate nominal power for a set of non-TCLs is obtained using the historical load profiles as

$$P_1 = \sum_{i=1}^{I} p_{1_i} \tag{6}$$

where P_1 is the aggregated nominal power for I heterogenous non-TCLs, and p_{1_i} is the nominal power for non-TCL i obtained using the historical load profiles.

The capacity of the aggregate TCL virtual battery is affected by the quantity and dynamics of the TCLs and the comfort preferences of the end users. The aggregate demand flexibility of the system increases as the number of TCLs increases. The slower the TCL dynamics are, the more flexible the set of TCLs are. Also, the higher the comfort bands are, the more flexible the set of TCLs are. The battery capacity for a single HVAC and WH is defined as in (7) and (8), respectively.

$$C_{HVAC} = \frac{\Delta_{HVAC}}{B_D \times P_{m_1}} \tag{7}$$

$$C_{WH} = \frac{\Delta_{WH} \times 60}{COP \times \Delta t \times P_{m_2}} \tag{8}$$

where C_{HVAC} and C_{WH} are the virtual battery capacities, Δ_{HVAC} and Δ_{WH} are the comfort bands for HVAC and WH units, respectively, and B_D is a coefficient extracted by discretizing the building model (1) into the intervals of Δt. The aggregate capacity for a set of HVAC and WH units is defined as

$$C = \sum_{i=1}^{N_1} C_{HVAC_i} + \sum_{j=1}^{N_2} C_{WH_j} \tag{9}$$

where C is the aggregate capacity of N_1 HVAC units and N_2 WH units. The capacity of the virtual battery represents the amount of aggregate flexibility of the HVAC and WH units. The level of charge of the virtual battery capacity is given by

$$b(t) = [b(t-1) + P(t-1) - P_0(t-1)] \times \delta \tag{10}$$

where $b(t)$ is the current level of charge, $b(t-1)$ is the level of charge at the previous time step, $P(t-1)$ is the power consumed at the previous time step, $P_0(t-1)$ is the nominal power at the previous time step, and δ is the battery dissipation rate. The difference between the power consumed and nominal power determines whether the virtual battery is being charged or discharged. When the power consumed is greater than the nominal power, the virtual battery is charged and the level of charge increases, and vice versa. The δ variable depends on the properties of the TCLs (e.g., insulation characteristics) and can be determined empirically. The level of charge can be converted to the state of charge (SOC) as

$$SOC(t) = \left(0.5 - \frac{b(t)}{2C}\right) \times 100\% \tag{11}$$

The $SOC(t)$ satisfies the following constraint:

$$0\% < SOC(t) < 100\% \tag{12}$$

Whether a power profile can be tracked by the total power consumption of a set of TCLs is determined by the minimum and maximum powers that the TCLs can consume. The minimum power that they can consume is zero, which simply occurs when all TCLs are turned off. On the other hand, the maximum power that they can consume occurs when all TCLs are turned on. Such limits lead to the following constraint:

$$0 \leq P(t) \leq \sum_{i=1}^{N} P_{m_i} \tag{13}$$

where P_{m_i} is the power rating of the *i*th TCL.

2.3 MODELING ENERGY MARKET USING A STACKELBERG GAME

The interaction between the DSO and multiple LAs in a day-ahead pricing market is designed as a Stackelberg game, where the DSO acts as the leader and LAs are regarded as the followers. In the defined game, the DSO determines the electricity price, while the LAs modify their consumption in response to the given price. The DSO aims to maximize its profit and social satisfaction while minimizing the peak

load, while the LAs aim to maximize their satisfaction and minimize their electricity cost. In order to ensure that the optimal power profile for each aggregator is feasible (i.e., the reference power profile generated from the game theoretic approach can be tracked and the temperature responses of the building TCLs stay within the comfort bands), the virtual battery is integrated into the game as a set of constraints for the LAs.

The Stackelberg game is applied using two types of electricity pricing structures: time-of-use (TOU) pricing and flat pricing. In the TOU pricing structure, the electricity prices vary according to the time of day. The DSO sets higher prices during the peak demand hours and lower prices during off-peak demand hours. In the flat pricing structure, the DSO sets a fixed electricity price throughout the day. For both pricing structures, it is assumed that all LAs are subject to the same prices set by the DSO.
The objective function of the DSO for the TOU pricing structure is defined as in (14). The function consists of three terms. The first term is the profit of the DSO, generated through buying electricity from the wholesale market and selling to the LAs. The second term represents the overall satisfaction of the DSO that changes parallel to the satisfaction of the LAs. The DSO should pay attention to the satisfaction of the LAs, which are its customers. Thus, the DSO takes care of the satisfaction of the LAs as part of a customer fulfillment strategy. Finally, the third term is the amount of peak load. The objective of the DSO is to maximize the first and second terms and minimize the third term while fulfilling the constraints given as follows:

$$\max_{p_t, l_{n,t}} U_{DSO} = \sum_{n,t} (p_t - c_t) \times l_{n,t} + S_{DSO} - \theta \times ST \times k \tag{14}$$

$$l_{n,t} = dr_{n,t} + hr_{n,t}, \forall_{n,t}$$

$$c_t \leq p_t, \forall_t$$

$$S_{DSO} = \sum_{n} S_{LA_n} \tag{15}$$

$$S_{LA_n} = \sum_{t} D_{n,t} \cdot \left(\frac{l_{n,t}}{D_{n,t}}\right)^{\alpha_{n,t}}, \forall_n \tag{16}$$

$$D_{n,t} = P_{0_{n,t}} + P_{1_{n,t}}, \forall_{n,t}$$

where p_t is the electricity price for all LAs at time t, c_t is the marginal cost of the electricity generation at time t, $l_{n,t}$ is the load of LA n at time t, which is the sum of the TCLs ($dr_{n,t}$) and non-TCLs ($hr_{n,t}$) power consumption, S_{DSO} is the overall satisfaction value of the DSO, which is the sum of the satisfaction values of all LAs as per in (15), ST is the number of time decision periods, k is the peak load, θ is a weighting coefficient to prioritize or deprioritize peak load reduction. The satisfaction value of LA n is computed as in (16) [51, 52], where $D_{n,t}$ is the nominal power of the LA n at time t, which is the sum of the nominal powers of TCLs and non-TCLs, and $\alpha_{n,t}$ is the sensitivity of LA n at time t towards consumption curtailment.

For the flat pricing structure, only the following additional equality is added to the aforementioned set of constraints to ensure the price does not vary throughout the day.

$$p_t = p_{t-1}, \forall_t$$

The objective function of the LAs is given as in (17). The function consists of two terms. The first term is the cost of electricity to the LAs. The second term is the satisfaction of the LAs. The satisfaction of the LAs reduces as the load of the LAs ($l_{n,t}$) deviates from the nominal power of the LAs ($D_{n,t}$). The LAs may prefer not to deviate much from their nominal loads as it might disturb the routine of end users. The

objective of the LAs is to minimize the first term and maximize the second term while fulfilling the constraints given as follows:

$$\min_{l_{n,t}} U_{LA} = \sum_t p_t \times l_{n,t} - S_{LA_n} \tag{17}$$
$$\underline{dr}_{n,t} \leq dr_{n,t} \leq \overline{dr}_{n,t}, \forall_{n,t}$$
$$\underline{hr}_{n,t} \leq hr_{n,t} \leq \overline{hr}_{n,t}, \forall_{n,t}$$
$$b_{n,t} = b_{n,t-1} + dr_{n,t-1} - P_{0_{n,t-1}}, \forall_{n,t}$$
$$b_{n,1} = b_{n,T} = 0$$
$$\left|b_{n,t}\right| \leq C, \forall_{n,t}$$
$$0.9 \times \sum_t P_{1_{n,t}} \leq \sum_t hr_{n,t} \leq 1.1 \times \sum_t P_{1_{n,t}}, \forall_n$$

where $\underline{dr}_{n,t}$ and $\overline{dr}_{n,t}$ are the minimum and maximum loads that the TCLs of LA n at time t can consume, respectively. Similarly, $\underline{hr}_{n,t}$ and $\overline{hr}_{n,t}$ are the minimum and maximum loads that the non-TCLs of LA n at time t can consume, respectively. The level of charge of the LA n at time t , $(b_{n,t})$ must be within the range of the aggregate capacity (9), which is equivalent to the SOC (11) being between 0% and 100%. The initial and end charge levels are assumed to be 0 (SOC = 50%). Note that the objective function of neither the DSO nor the LAs includes any parameters (e.g., K_1 and UA) from the mathematical models that are used for simulating the HVAC and WH units. This shows that the proposed approach is model free and does not require any mathematical modelling and/or model training.
The Stackelberg game is solved using the backward induction method [51, 53], which follows two main steps. First, it derives the optimal load $l^*_{n,t}$ by computing the first-order derivative of LAs' objective functions (17). Second the optimal load, $l^*_{n,t}$, computed using (18), is plugged into the objective function of the DSO (14). This operation converts the bi-level optimization problem into a single level optimization problem, in which the price p_t is the only variable. The backward induction method is simple yet effective method and scalable to any number of LAs.

$$l^*_{n,t} = D_{n,t} \times \left(\frac{p_t}{\alpha_{n,t}}\right)^{\frac{1}{\alpha_{n,t-1}}}, \forall_{n,t} \tag{18}$$

In addition, the Stackelberg game in (14)-(17) can be solved in a distributed way (to preserve privacy and reduce computational complexity) using any of the distributed solving methods such as particle swarm optimization (PSO) [54], pattern search algorithm (PSA) [54], or collaborative optimization (CO) [55].

2.4 POWER ALLOCATION OF BUILDING TCLS USING MEDEL-FREE CONTROL

The control of the end-user TCLs is not a simple task because of their large scale, heterogenous nature, and sometimes uncertain behavior. The controller has to determine the TCL units that need to be powered on from a large number of units. Also, the controller needs to track the optimal power profile closely to ensure that the outcomes anticipated by the DSO and LAs can be realized. Failure to do so may cause significant discomfort, severe financial losses, and/or poor grid stability. Thus, the selection and design of the controller is crucial. For this reason, the MFC is utilized for the control of the end-user loads.

MFC is a control mechanism that does not require any modeling effort for the various building TCLs such as HVAC systems, WHs, and others. It is based on approximating the TCL by an ultra-local model as [43]:

$$\dot{y} = F + \sigma u \tag{19}$$

where u is the input power (or on/off state) of the TCL system, $\dot{y}$ is the rate of change in the indoor/water temperature of the TCL system, and F describes the poorly known or unknown parts of the TCL system. The parameter σ is to correct the difference in the magnitudes of the input and the output. Equation (19) should not be confused with a "black box model" of the TCL system. In MFC, (19) is updated at each timestep from the knowledge of the input-output behavior of the unmodeled TCL system in order to estimate the quantity F, which is approximated by a piecewise constant function given as [56]:

$$F = \frac{-6}{L^3}\int_{t-L}^{t} [(L - 2\tau)y(\tau) + \sigma\tau(L - \tau)U(\tau)]d\tau \tag{20}$$

Note that F is estimated using the measurements of the system obtained in the last L seconds, and it is being updated accordingly. Unlike the classic proportional–integral–derivative (PID) controllers, MFC continuously updates the local model (F) in (20) via the unique knowledge of the input-output behavior for both linear and nonlinear systems. For this reason, MFC has shown to overperform the classic PID controllers and many others including fuzzy and neuro-fuzzy controllers [57, 58]. Based on the numerical knowledge of F, the control is computed using (21) as a simple cancellation of the nonlinear terms, as described in F, in addition to a closed loop tracking of a reference trajectory. More specifically, using the latest F, the intelligent proportional control law is given by [59]:

$$u = -\frac{F - \dot{y}^* + K_p(y - y^*)}{\sigma} \tag{21}$$

where y^* is the desired reference trajectory (TCL temperature set point), and K_p is the proportional control gain. Combining (19) and (21) provides the error dynamics as:

$$\dot{r} + K_p r = 0 \tag{22}$$

where $r = y - y^*$ is the tracking error and F does not appear anymore. The solution of the first-order differential equation in (22) is given as:

$$r(t) = r(t_0)e^{-K_p(t-t_0)} \tag{23}$$

where t_0 is the initial time. Equation (23) shows that the tracking error asymptotically decays to 0 for $K_p > 0$, which guarantees the asymptotic stability of the system and makes the tuning of the proportional gain straightforward. Thus, the tracking condition can be easily achieved by setting the value of K_p to be the solution of (23) as:

$$K_p = \frac{log\, r(t_0) - log\, r(t)}{t - t_0} \tag{24}$$

Note that K_p is updated at every timestep according to (24). As a result, σ and L are the only two parameters to be tuned, and their selection is also straightforward. A sufficiently small value is needed for the parameter L, and σ can be determined from collected input-output measurements as $\sigma = \dot{y}/u$. This makes the control design simple to implement. The asymptotic stability criterion in addition to the closed form solution of the control gain K_p for MFC make it more intelligent and beneficial than the classic PID controller.

In summary, MFC is employed in this project because it has the following main characteristics:

a) It does not require any modeling effort for the various building TCLs and their disturbances.

b) It is straightforward to tune, in contrast to the commonly used classic PID controllers that are very challenging to tune (usually depends on trial-and-error methods).

c) It is asymptoticly stable, in contrast to the classic PID controllers.

d) It is very simple to implement in real time since it requires very light computations.

The additional power allocation and power tracking constraints in the MFC design are imposed using Algorithm 1, which works similar to the priority-based control algorithm in [46]. The only difference is that, instead of the priorities determined based on TCL temperature deviations, Algorithm 1 uses the control input u values (power inputs) to determine the units to be turned on or off.

Algorithm 1 Power Allocation of building TCLs for LA n

1: FOR every time step, t
2: FOR every TCL j with rated power of $P_m(j)$
3: Compute u using (21)
4: Sort u values in descending order and get the rank r of TCLs
5: Initialize as $P_{consumed} = 0$ and $r = 1$
6: WHILE $P_{consumed} \leq dr_{n,t}$
7: Find the TCL j with the rank of r
8: Turn on the TCL j
9: $P_{consumed} := P_{consumed} + P_m(j)$
10: $r := r + 1$
11: Simulate the TCLs using (1), (2), and (4)

2.5 NUMERICAL CASE STUDY

A large-scale case study is presented in this section to demonstrate the performance of the proposed hierarchical model-free transactional control approach with ten LAs and 10,000 heterogenous building TCLs and 10,000 non-TCLs. Each LA includes 1000 TCL and 1000 non-TCL units. For the TCL units, a random set of numbers adding up to 1000 is considered for the numbers of residential HVAC, commercial HVAC, and WH units. For the non-TCL units, two prototype building models provided by the U.S. Department of Energy are considered [60]. The non-TCL units include 500 single-family and 500 medium office buildings.

The properties of the TCLs are summarized in Table I. As shown in the table, some properties of the HVAC and WH units are randomized within 20% range to further differentiate the LAs.

In the case study, the Stackelberg game is conducted hourly, while the control of the TCLs using MFC is conducted at 10-minute intervals. Accordingly, the case study includes three main steps. First, the hourly nominal power profiles are generated using the day-ahead forecasts of the external temperature, solar radiation, and hot water usage profiles, and the corresponding battery constraints are determined for each LA. Second, as a result of the Stackelberg game, an optimal power profile and a price signal are generated for each LA. In computing the optimal power profiles, four different scenarios are considered. Table II summarizes the scenarios considered for the optimization. The scenarios aim to capture the impacts of the pricing strategy (e.g., flat and TOU) and the peak load reduction weight (θ) on the resulting optimal loads. Third, the obtained power profiles are allocated across the different building TCLs using the MFC every 10-minute time intervals.

Figure 3 shows the disturbances, including weather conditions and hot water usage profiles that the LAs are subjected to. The nominal power profiles and the battery constraints of the LAs are computed

accordingly and passed to the Stackelberg game model. The outdoor weather conditions including temperature and solar radiation data are taken from the typical meteorological year 3 (TMY3) weather data of Las Vegas [61]. The hot water usage profile data are taken from a single-family detached house [62]. Prior to the case study, both outdoor weather conditions and hot water usage data profiles are converted into hourly intervals.

TABLE I. TCL properties.

Parameter	Residential HVAC	Commercial HVAC	Water Heater	Range
P_m	3.5 kW	11.0 kW	4.5 kW	N/A
K_1	0.8 kW/℃	2.4 kW/℃	N/A	±20%
K_2	5.4 kW/℃	16.2 kW/℃	N/A	±20%
K_3	0.2 kW/℃	0.7 kW/℃	N/A	±20%
K_4	1.5 kW/℃	4.5 kW/℃	N/A	±20%
K_5	1.1 kW/℃	3.4 kW/℃	N/A	±20%
C_1	45 MJ/℃	140 MJ/℃	N/A	±20%
C_2	140 MJ/℃	440 MJ/℃	N/A	±20%
C_3	30 MJ/℃	100 MJ/℃	N/A	±20%
COP	4	4	1	N/A
γ	0.15	0.15	N/A	N/A
UA	N/A	N/A	0.07 Btu/min	±20%
T_{fresh}	N/A	N/A	21.0℃	N/A
$T_{ambient}$	N/A	N/A	20.5℃	N/A
V	N/A	N/A	250 l	N/A

P_m: rated power, K_1: thermal conductivity of ceiling, K_2: thermal conductivity of floor, K_3: thermal conductivity of windows, K_4: thermal conductivity of external walls, K_5: thermal conductivity of internal walls, C_1: heat capacity of air, C_2: heat capacity of internal walls, C_3: heat capacity of external walls, COP: coefficient of performance, γ: solar heat gain coefficient, UA: standby loss, T_{fresh}: intake water temperature, $T_{ambient}$: ambient temperature of the room where water heater located, and V: tank volume.

TABLE II. Optimization scenarios.

Scenario	Pricing Structure	θ
1	Flat	10
2	Flat	20
3	TOU	10
4	TOU	20

Figure 4 shows the hourly α values assumed for computing the satisfaction values of the LAs as per in (16). The higher the value of α, the less conservative the LAs to their satisfaction. By altering the α values, the potential variability that can occur in the preferences of the LAs are taken into account.

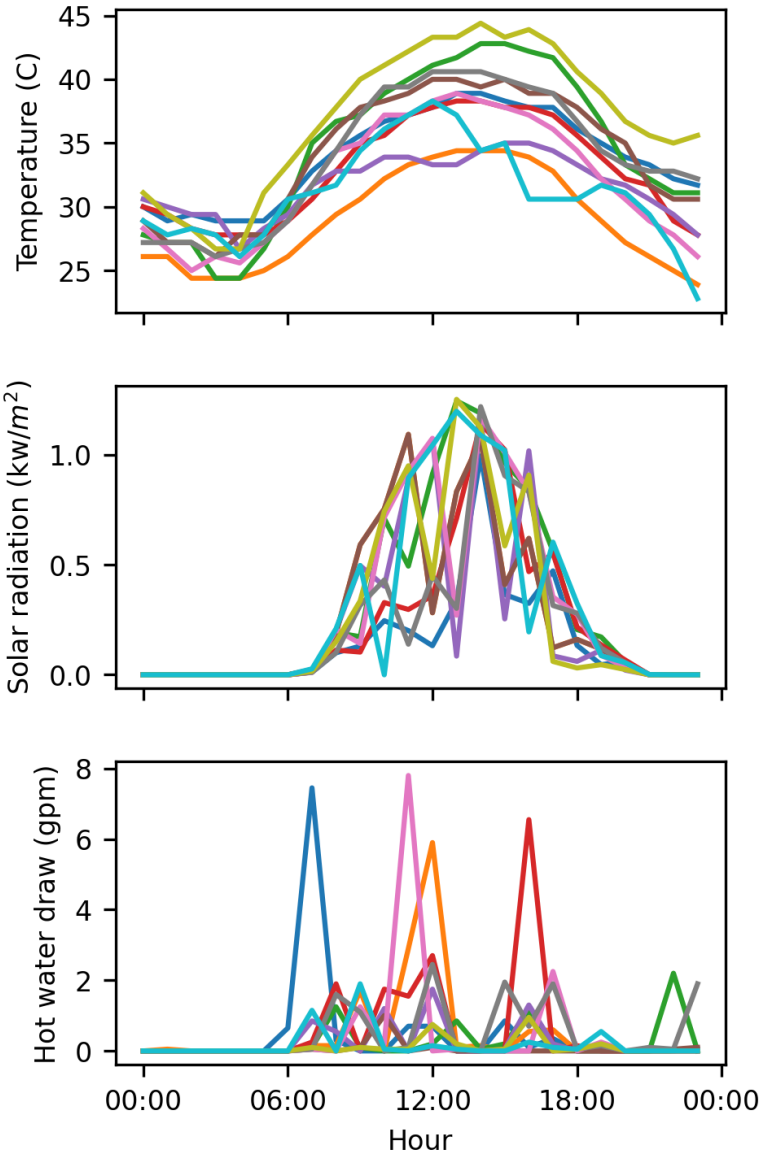

Figure 3. Disturbances for the numerical case study.

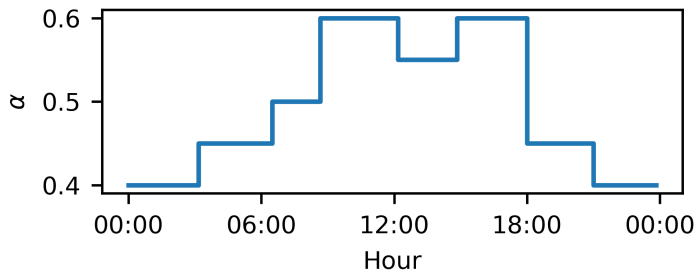

Figure 4. The α values used for computing the satisfaction of LAs.

Figure 5 shows a comparison of hourly nominal and optimal power profiles for the four scenarios. It is observed that the scenarios with flat pricing (i.e., Scenarios 1 and 2) are not successful in reducing the peak load. However, the scenarios with TOU pricing (i.e., Scenarios 3 and 4) achieve significant amount of peak load reduction. The peak loads are 82.51 MW and 71.92 MW for Scenarios 3 and 4, respectively, as compared to the peak loads of 108.20 MW and 95.69 MW for Scenarios 1 and 2, respectively. This shows that the proposed Stackelberg game is able to optimize the power profiles for TOU pricing by shifting loads from peak to off-peak hours, and that the weight of load reduction is useful in prioritizing or deprioritizing the objective of peak load reduction.

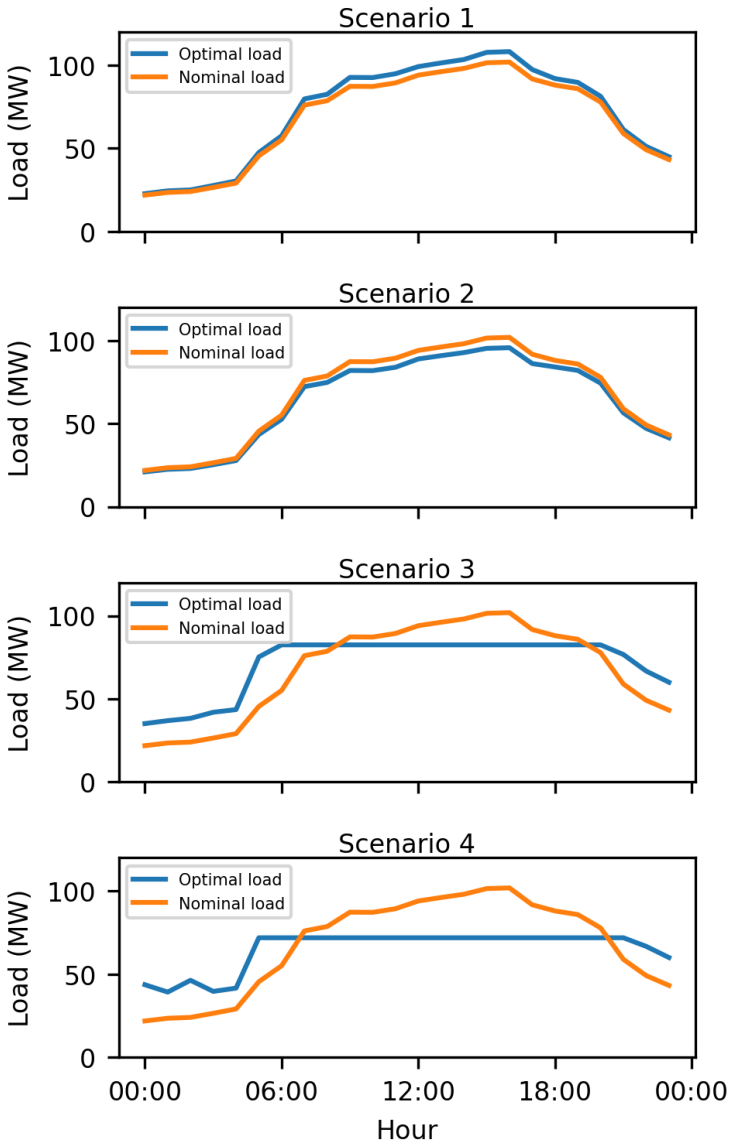

Figure 5. Nominal and optimal power profiles for different scenarios.

Figure 6 shows the electricity prices across the different scenarios and the marginal cost of electricity. Scenarios 3 and 4 set higher prices between 12:00 and 18:00 to reduce the peak load occurred during this period. Overall, the prices in Scenario 4 are higher than the prices in Scenario 3, because Scenario 4 gives more importance to peak load reduction and therefore sets more aggressive prices. Likewise, Scenario 1 sets a lower price than Scenario 2, because Scenario 1 gives less importance to peak load reduction.

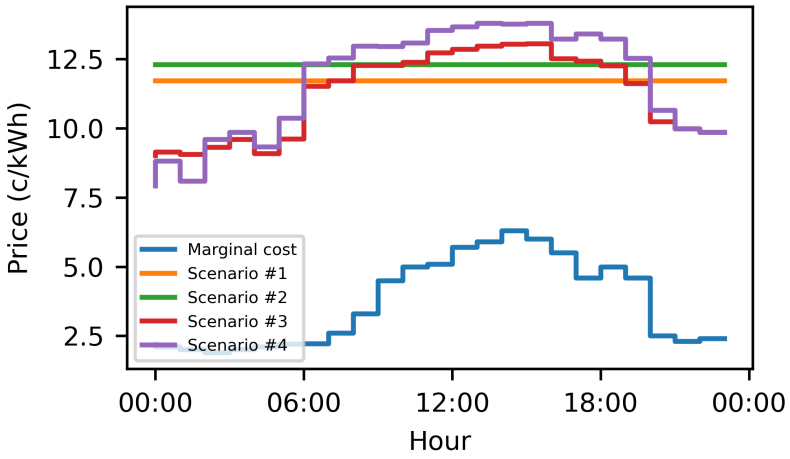

Figure 6. Marginal cost of electricity generation and optimal price signals.

Table III compares the overall results for the DSO and LA 1. For all scenarios, TOU pricing achieves higher peak load reduction than flat pricing, which shows the effectiveness of the TOU pricing structure in DR. Scenarios 1 and 3 result in more profit but higher peak loads. This shows the tradeoff between profit and peak load reduction from the DSO perspective. Scenarios 2 and 4 cost less to LA 1, because these scenarios attach more importance to peak load reduction, and therefore the DSO incentivizes LAs more to modify their consumption. The results for the other nine LAs are similar and therefore not included in the table for the sake of conciseness.

TABLE III. Results of the Stackelberg game.

Objective	Scenario 1	Scenario 2	Scenario 3	Scenario 4
DSO Profit	$128,371	$125,033	$129,625	$126,087
DSO Satisfaction	369,423	225,935	404,451	292,971
Peak Load	108.20 MW	95.69 MW	82.51 MW	71.92 MW
LA 1 Cost	$20,785	$19,686	$20,428	$19,336
LA 1 Satisfaction	41,336	39,242	41,188	39,164

Figure 7 shows the resulting temperature responses for the optimal load profile for LA 1 in Scenario 4. The MFC was able to maintain temperatures within the comfort bounds for the given reference power profile with no prior information about the HVAC and WH units. Similarly, temperature responses for all scenarios and LAs are within the bounds. For this reason, only the results shown in Figure 7 are presented here.

The case study also shows that MFC is a very computationally efficient algorithm and can be deployed for very small-time scales. Specifically, each iteration (time step) run for MFC requires 3 milliseconds to make control decisions using Matlab on a standard four-core personal computer, while it requires 600 milliseconds for the traditional model-predictive control (MPC) [63]. Thus, MFC is 200 times faster. Such attribute makes MFC an ideal controller for real-time or near real-time DR applications.

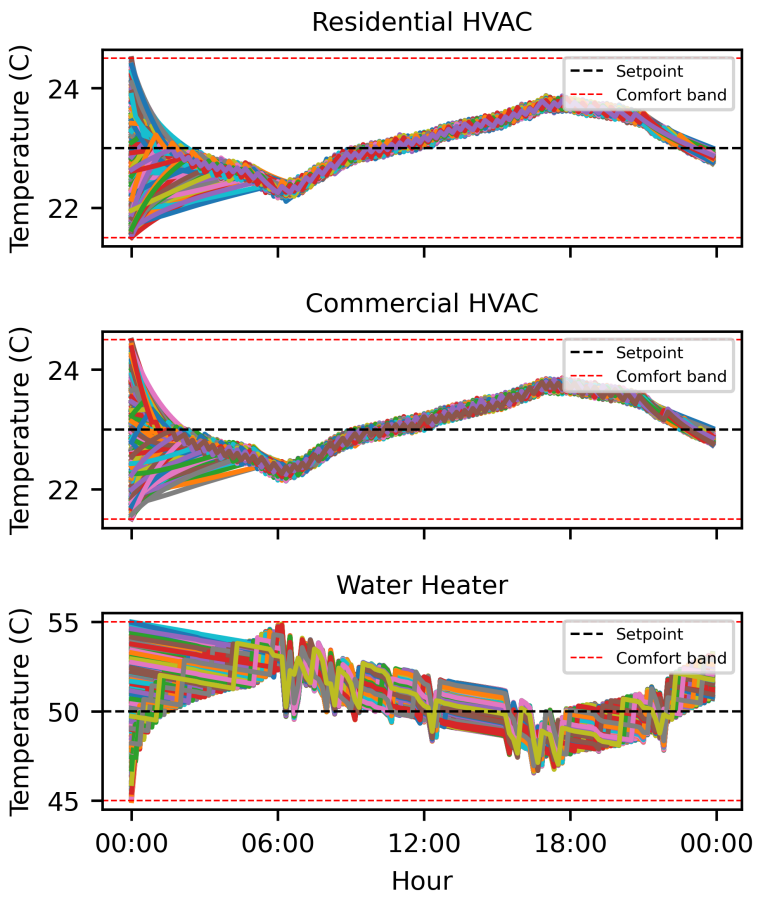

Figure 7. Resulting temperature responses for the optimal load in LA 1 for Scenario 4.

In terms of power allocation and tracking, MFC ensures the aggregate power consumption of LAs to closely follow the reference optimal power profiles. Figure 8 shows the tracking performance of the MFC for LA 1 of Scenario 4. Please note that the MFC takes control after 20 minutes because MFC uses the previous 20 minutes of measurements before starting to make decisions. So, there is no control in the first 20 minutes of the simulation.

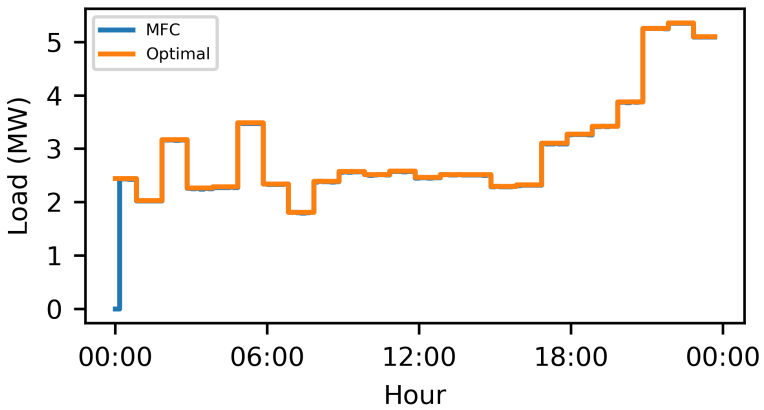

Figure 8. Tracking performance of MFC in LA 1 for Scenario 4.

Figure 9 shows the changes in the SOC of the virtual battery in LA 1 for Scenario 4. The virtual battery is charged until 6:00 as the optimal load is greater than the nominal load. Consequently, residential and commercial buildings' indoor temperatures decrease, and WH temperatures increase. After that the optimal load is less than the nominal load and the virtual battery is discharged until 18:00. In this period, residential and commercial buildings' indoor temperatures increase, and WH temperatures decrease. Finally, the virtual battery is charged again until 00:00. As shown in the figure, the battery constraints are never violated and therefore the temperatures stay in bounds.

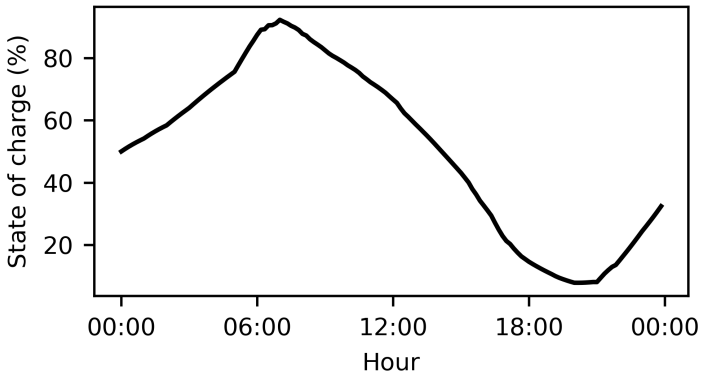

Figure 9. The SOC of the virtual battery in LA 1 for Scenario 4.

3. THE STOCHASTIC HIERARCHICAL MODEL-FREE TRANSACTIONAL CONTROL APPROACH

In this section, we have modelled the uncertainties with respect to the wholesale market prices and aggregated nominal loads of LAs by stochastic programming. The building level temperature preference is guaranteed by the virtual battery constraints in the model derived from the building thermal properties. In Section **Error! Reference source not found.**, the stochastic game model for the DSO and LAs is presented, a nd several case studies are shown in Section **Error! Reference source not found.** to demonstrate the effectiveness of the proposed model in preserving the benefits of both parties with uncertainties while maintaining the desired temperature range at the building level.

3.1 STOCHASTIC PRICING-DEMAND GAME

In the proposed DR pricing game, all the parameters and variables are listed in Table IV, followed by the mathematical model.

Table IV. Notations for the stochastic game model.

Index	
T, t, n, s	Decision period, index for hours, LAs and scenarios
Parameters	
$C_{s,t}, \overline{P}$	Marginal cost of electricity generation, price upper bound
$\underline{L}_{n,t}, \overline{L}_{n,t}$	Lower bound, upper bound of demand limit for LAs
$Dh_{s,n,t}, Dd_{s,n,t}$	Nominal thermal demand, non-thermal demand of LAs
$\alpha_{n,t}, \theta$	Satisfaction preferences of LAs, penalty coefficient for peak load
BI, ϵ	Initial State-of-Charge (SOC), dissipation rate of virtual battery
$\underline{B}_{n,t}, \overline{B}_{n,t}$	Lower bound, upper bound of state of charge for virtual battery
Variables	
$p_t, dl_{s,n,t}$	Resulted electricity price, total electricity load of each LA
$hr_{s,n,t}, dr_{s,n,t}$	Resulted thermal load, non-thermal load of each LA
$m_s, b_{s,n,t}$	Peak load, current level of charge in virtual battery

In the Stackelberg game, the DSO is the leader with the privilege of setting the price signal. Its objective is to maximize the profit in (25), taking the overall satisfaction from LAs (the third term in (25)) and peak load penalty (the fourth term in (25) into account). Due to the uncertainties, the objective function is in its expectation form (product summation of the scenarios and their probabilities). The electricity price is limited by the marginal cost C and allowable upper limit in any scenario (as described in the constraint (26)). Equation (27) is used to define the peak load, which should be the maximum total load for the whole duration.

$$DSO{:}\max U_o = \sum_s prob_s \cdot \left(\sum_{n,t} p_t \cdot dl_{s,n,t} - \sum_{n,t} C_{s,t} \cdot dl_{s,n,t} + \sum_{n,t} S\left(Dl, dl\right) - \theta \cdot T \cdot m_s \right) \qquad (25)$$

$$C_{s,t} \le p_t \le \overline{P},\ \forall s,t \tag{26}$$

$$m_s \ge \sum_n d\,l_{s,n,t},\ \forall s,t \tag{27}$$

LAs are the followers in the game that respond to the price signal from the leader and adjust the electricity consumption to maximize their own utility functions in (28). Similar to (25), the objective function in (28) is in the expectation form. The function $S(Dl, dl)$ is used to represent the monetary value of the customers' satisfaction. When the actual consumption after demand response is equal to its nominal demand, the satisfaction value is defined to be 1 as illustrated in Figure 10. $S(Dl, dl) = (Dl_{s,n,t}) \cdot w_{n,t} \cdot (\frac{dl_{s,n,t}}{Dl_{s,n,t}})^{\alpha_{n,t}}$ which is revised based on [52], and it keeps the convex property. Note that $Dl_{s,n,t} = Dh_{s,n,t} + Dd_{s,n,t}$ is the total nominal load; w is a user defined parameter; α represents the sensitivity of demand shifting, which is usually higher during peak hours. On the other hand, the electricity price during peak hours is also higher, and therefore, the feasibility and the quantity of load reduction during peak hours greatly depends on the trade-off potential between the occupants' comfort level and monetary expense.

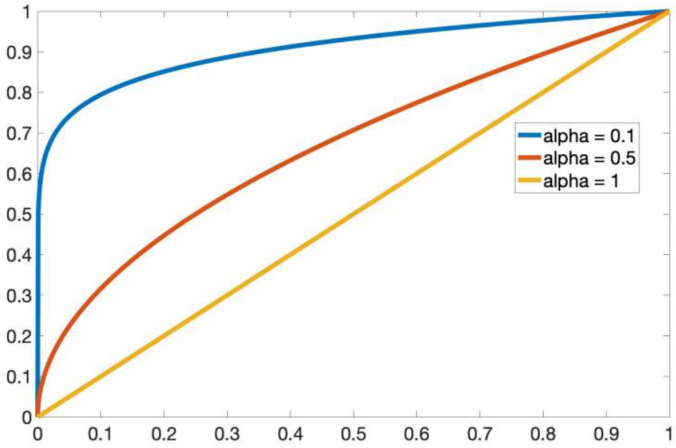

Figure 10. The normalized customer satisfaction value (y-axis) for different α (x-axis: $\frac{dl}{Dl}$).

Equation (29) calculates the resulting total consumption by summing up the thermal load hr and the non-thermal load dr. Equation (30) limits the hourly non-thermal demand, and (31) uses the range $\pm 10\%$ to ensure that the daily non-thermal load does not fluctuate too much for the required daily work. The stricter equality constraint $\sum_t d\,er_{n,t} = \sum_t D\,d_{n,t}$ could be an alternative to (31), which means no curtailment on the daily non-thermal consumption is allowed.

$$LAs{:}\max U_n = \sum_s prob_s \cdot \left(\sum_t S\,(Dl, dl) - \sum_t p_t \cdot dl_{s,n,t} \right) \tag{28}$$

$$dl_{s,n,t} = hr_{s,n,t} + dr_{s,n,t},\ \forall s,n,t \tag{29}$$

$$\underline{L}_{n,t} \le dr_{s,n,t} \le \overline{L}_{n,t},\ \forall s,n,t \tag{30}$$

$$0.9 \cdot \sum_t D\,d_{s,n,t} \le \sum_t d\,r_{n,t} \le 1.1 \cdot \sum_t D\,d_{s,n,t},\ \forall s,n,t \tag{31}$$

$$\underline{B}_{n,t} \le b_{s,n,t} \le \overline{B}_{n,t},\ \forall s,n,t \tag{32}$$

$$b_{s,n,t} = \epsilon \cdot \left(b_{s,n,t-1} + hr_{s,n,t} - Dh_{s,n,t}\right),\ \forall s,n,t \tag{33}$$

Equations (32) and (33) constrain the levels of charge of the virtual batteries for the aggregated buildings, which are derived based on the building thermal characteristics. The difference between the actual power consumed hr by thermal appliance and the nominal thermal load Dh determines whether the virtual battery is being charged or discharged. ϵ is the virtual battery dissipation rate, which depends on the properties of the thermal load (e.g., insulation characteristics) and can be empirically determined. For further details on developing the virtual battery constraints, readers are referred to Section 2.2.

To convert the bi-level game into the single model, the classical BI method (centralized approach) is adopted and can be broken down into the following the two steps. First, derive the optimal DR to the price. Assume the electricity price p_t is provided as a parameter from the DSO, then the best load response $dl^{\star}_{s,n,t}$ can be obtained by the first-order derivative of the LAs' objective functions, as in (34).

$$dl^{\star}_{s,n,t} = \left(\frac{p_t}{w_{n,t} \cdot \alpha_{n,t}}\right)^{\frac{1}{(\alpha_{n,t}-1)}} \cdot (Dd_{s,n,t} + Dh_{s,n,t}) \tag{34}$$

Second, derive optimal price based on the user response. After the optimal DR is obtained, the price can then be expressed using $dl^{\star}_{s,n,t}$ and plugged into the upper level with the other additional lower-level constraints. The resulting single level model requires all the parameter information from LAs and is solved by the DSO in a centralized way.

3.2 NUMERICAL CASE STUDY

In the proposed stochastic model, the uncertainties arise from the nominal thermal demand Dh, the nominal non-thermal demand Dd, and the marginal cost of electricity generation C. The nominal non-thermal demand is adopted and mixed based on the commercial building reference load from the U.S. Department of Energy in [60] and the marginal cost data in [52]. Without loss of generality, a uniform distribution is assumed for non-thermal demand and marginal cost, and the scenarios are sampled within a certain range based on the reference value for each hour. Scenarios of the nominal thermal demand are simulated based on different weather conditions.

Ten LAs are considered in this study, and each one has three types of total 1000 heterogeneous thermal loads: residential HVAC, commercial HVAC, water heaters. Initially, 200 scenarios are generated for each of the three uncertain parameters Dh, Dd, C. To achieve a computational tractability while capturing the main stochastic information of the random distribution embedded in the original scenario set as much as possible, a simultaneous backward method [64, 65] is applied to reduce the number of deteriorated scenarios. This is explained in the following steps:

- Step 1: Set S as the initial set of scenarios, DS is the scenarios to be deleted. Initial DS is empty. Compute the distances $DT_{s,s'}(s, s' = 1, \dots, N)$ of all scenario pairs.
- Step 2: For each scenario k, the distance $DT_k(r) = \min DT_{k,s'}.\, s', k \in S, s' \neq k.\, r$ is the scenario index that has a minimum distance with scenario k.
- Step 3: Compute the distance in the probability sense $PD_k(r) = p_k \cdot DT_k(r), k \in S$. Choose d so that $PD_d = \min PD_k, k \in S$.
- Step 4: Delete scenario d: $S = S - \{d\}, DS = DS + \{d\}, p_r = p_r + p_d$. And repeat until the remaining scenario number meets requirement.

Eventually, 20 scenarios of the three uncertain parameters are resulted from the reduction process and the probability for each scenario has been updated by Step 4. The nominal thermal load scenarios are shown for LA 1 and LA 10 in Figure 11. The nominal non-thermal load scenarios and marginal cost scenarios are shown in Figure 12. The α parameter in the satisfaction function and probabilities of the 20 scenarios are shown in Figure 13.

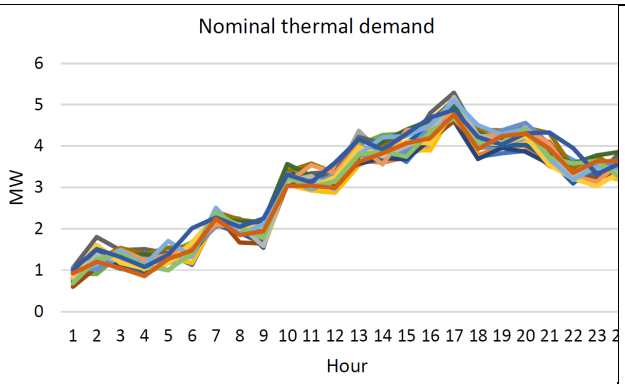

(a) Nominal thermal load of LA 1.

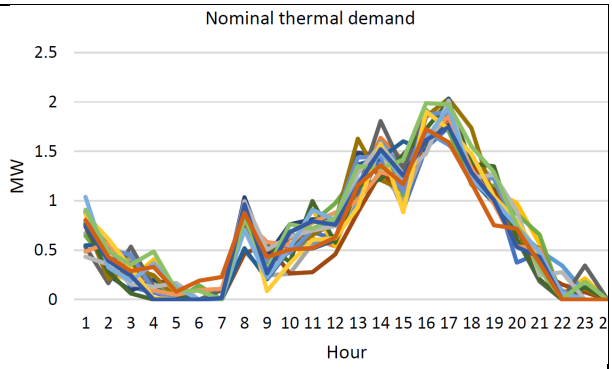

(b) Nominal thermal load of LA 10.

Figure 11. The nominal thermal load for LAs 1 & 10 for the resulted 20 scenarios.

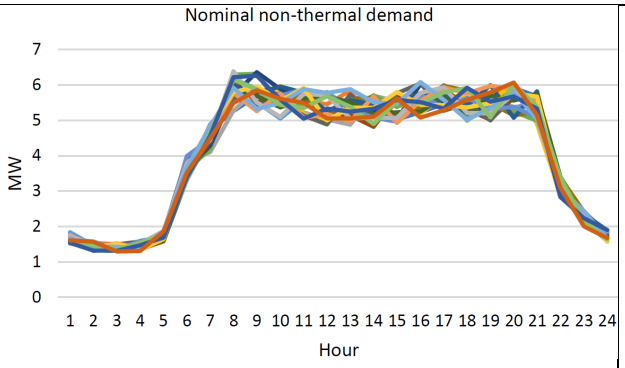

(a) Nominal non-thermal load of LA 1.

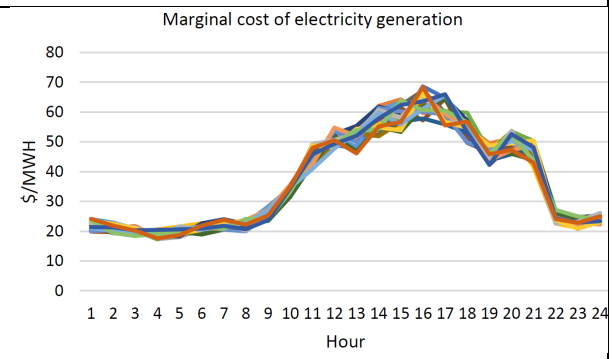

(b) Marginal cost of electricity generation.

Figure 12. The nominal non-thermal load of LA 1 and marginal cost of electricity generation for the resulted 20 scenarios.

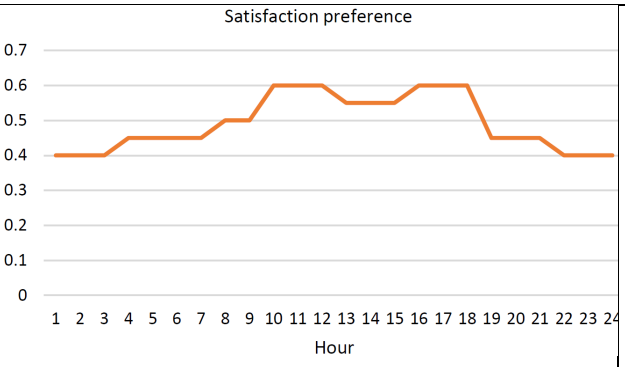

(a) α parameter in the satisfaction function.

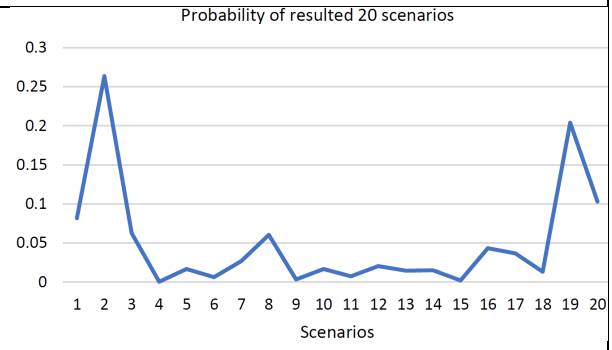

(b) Probability of the resulted 20 scenarios.

Figure 13. The α parameter and probability value of the resulted 20 scenarios.

To illustrate the effectiveness of the proposed stochastic model in the peak load reduction for the DSO, two groups of experiments are conducted with penalty coefficients of peak load $\theta = 10$ and $\theta = 20$. Electricity price is the decision variable of the DSO at the upper level which needs to be determined regardless of the uncertainty scenarios in the LAs' model. When the penalty on peak load is higher, the resulted electricity price is also higher in overall as shown in Figure 14(a). The peak load reduction is demonstrated in Figure

14(b), indicating that the 100 MW peak in the nominal total demand is reduced to about 80 MW in all 20 scenarios by shifting it to early morning or late night.

Take LA 1 as an example, the peak load (at about hour 17) of its aggregated nominal thermal load in Figure 14(a) has shifted to about hour 7 and hour 24 in Figure 15(a) in the optimized results. The underlying reason is that shifting the peak of thermal load could reduce overall peak load in Figure 14(b) which benefits the DSO. Also, since the resulted price is lower at hour 7 and hour 24, the electricity cost will be lower for the LAs without sacrificing comfort level, which is ensured by the virtual battery constraints.

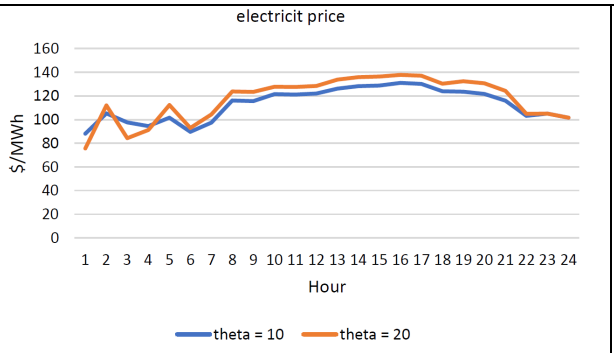

(a) Optimum electricity price resulted from stochastic gaming model.

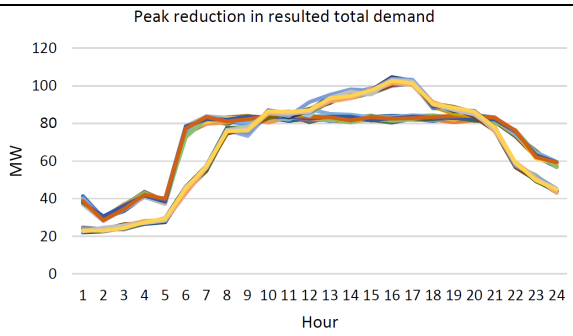

(b) Peak reduction from the nominal total demand for 20 scenarios with θ= 10.

Figure 14. The resulted optimal electricity price and total demand (thermal & non-thermal) of all LAs in each scenario.

As for the cooling case here, a fully charged battery means that the temperatures of the thermal loads are less than the setpoint temperatures as much as the comfort band limits. Shown by the virtual battery level of LA 1 in Figure 15(b), it charges before hour 7 as the resulted thermal load in Figure 15(a) is overall higher than its nominal thermal load in Figure 11(a), therefore its HVAC temperatures in Figure 16(a) also drops below the setpoint. Then, the virtual battery starts to discharge during hour 8 and hour 20 as the resulted thermal load is lower that its nominal load in this period and accordingly the HVAC temperatures raise. At the last several hours 20-24, the resulted thermal load of LA 1 in Figure 15(a) is above 4 MW, which is higher than its nominal thermal load in Figure 11(a) again, and thus the virtual battery level starts to charge again and indoor temperature goes down. Other aggregators like LA 10 shows a similar pattern in Figure 17. Scenario 2 is chosen to illustrate the building temperature responses of LAs in Figure 16 and Figure 17 as it has the highest occurrence probability (about 0.27) out of the final 20 scenarios, also the initial temperatures of all thermal loads are uniformly distributed within the temperature band.

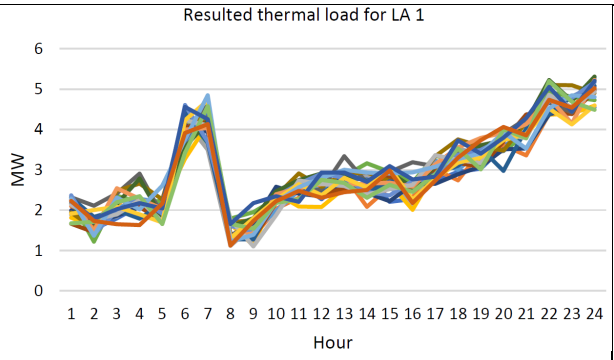

(a) Optimal thermal load for LA 1 under each scenario with θ = 10.

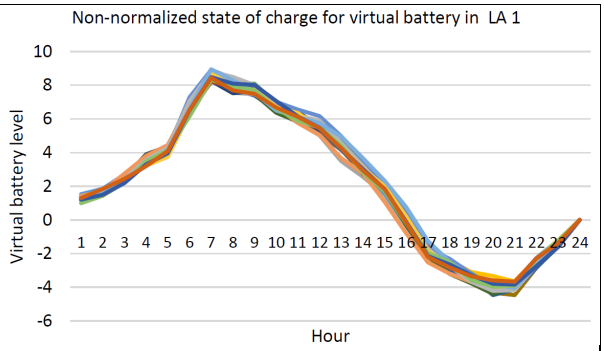

(b) Virtual battery level for LA 1 under each scenario with θ = 10.

Figure 15. The resulted thermal load and virtual battery level for LA 1 under each scenario.

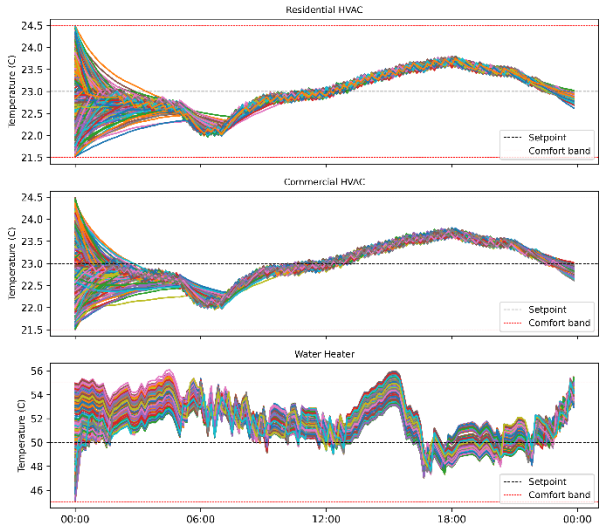

(a) Temperature responses of LA 1 with $\theta = 10$ under Scenario 2.

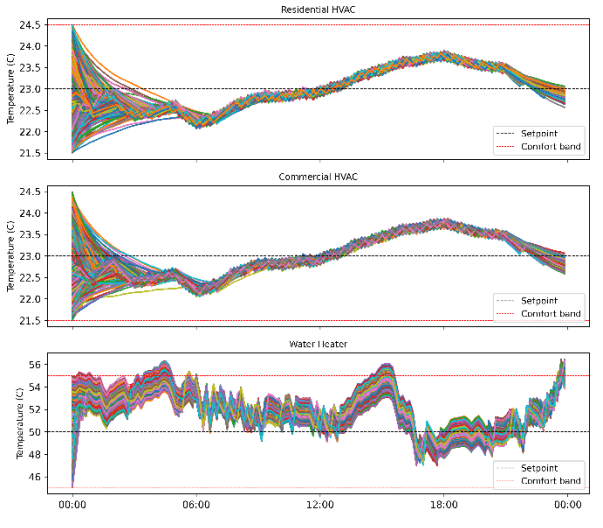

(b) Temperature responses of LA 1 with $\theta = 20$ under Scenario 2.

Figure 16. The temperature responses of LA 1 under Scenario 2.

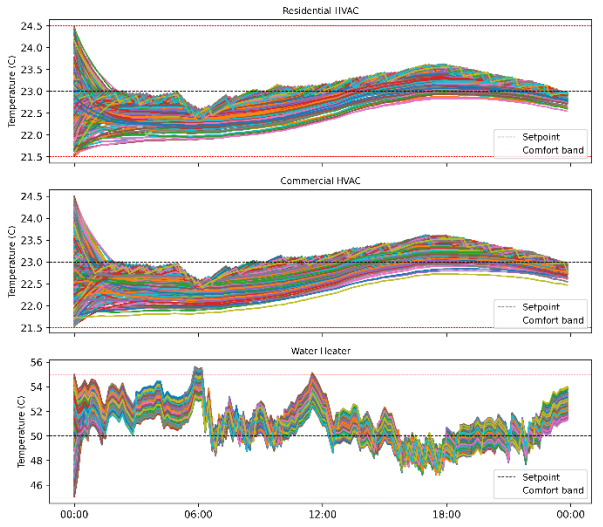

(a) Temperature responses of LA 10 with $\theta = 10$ under Scenario 2.

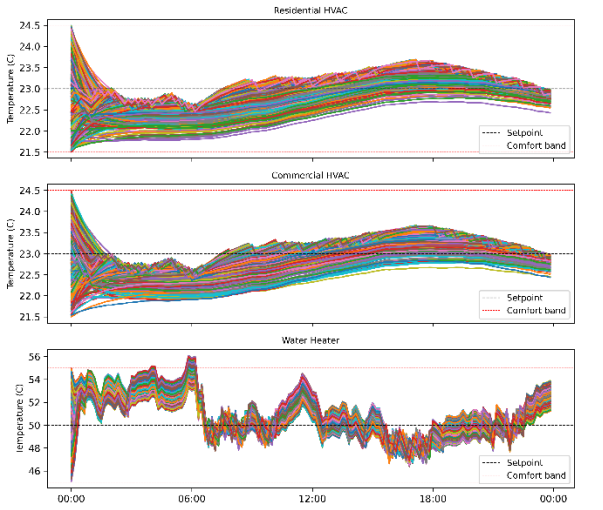

(b) Temperature responses of LA 10 with $\theta = 20$ under Scenario 2.

Figure 17. Temperature responses of LA 10 under Scenario 2.

Besides the peak reduction benefit for the DSO, the proposed stochastic pricing-demand response model could also benefit LAs on the cost saving with a trade-off on electricity consumption satisfaction. To demonstrate such trade-off, another group of experiments is added: the electricity price is assumed to be flat for the whole day. To realize the flat price, one additional constraint $p_{t-1} = pt, t \geq 2$ is added to the upper level of the proposed model. Since there are multiple scenarios with different probabilities, the expected results for some main metrics are summarized into Table V. LAs 1 & 10 are also used here as an example, and the results for all other load aggregators have a similar pattern.

Table V. Profit and cost in different groups of experiments considering uncertainties.

DSO level	**Flat ($\theta = 10$)**	**Flat ($\theta = 20$)**	**TOU ($\theta = 10$)**	**TOU ($\theta = 20$)**
Expected Peak Load	108.68	95.99	83.48	73.47
Expected PAR value	1.53	1.50	1.18	1.13
Expected DSO revenue	199365	188606	195242	185349
Expected DSO cost	72477	64990	67059	60364
Expected DSO profit	126888	123616	128183	124984
Aggregator level	**Flat ($\theta = 10$)**	**Flat ($\theta = 20$)**	**TOU ($\theta = 10$)**	**TOU ($\theta = 20$)**
Expected average price of LA1	117.13	123.09	114.84	118.93
Expected average price of LA10	117.13	123.09	115.53	119.49
Expected bill payment of LA1	20978	19862	20635	19605
Expected bill payment of LA10	14602	13803	14271	13536
Expected satisfaction of LA1	41817	39688	41638	39732
Expected satisfaction of LA10	28618	27114	28310	26971

In Table V, the expected average price for each LA is calculated by $(\sum_s \mathrm{prob}_s \cdot \sum_t p_t \cdot dl_{s,n,t})/(\sum_s \mathrm{prob}_s \cdot \sum_t dl_{s,n,t})$. As observed, under the same price structure (flat or TOU), higher penalty on peak load results in higher average price, which means the cost for LAs to consume one unit electricity is higher, and the TOU price has more advantage in lowering the average electricity price with the same peak penalty level. Meanwhile, the PAR (peak-to-average ratio) value is depressed lower along with a higher peak penalty level, the DSO has a slight lower profit in return of lower peak penalty which is more critical in stabilizing the power grid. The trade-off between satisfaction and bill payment for LAs can also be observed, for instance, the satisfaction decreases from flat price to TOU price due to the load shifting, but bill payment is also lower as more electricity is consumed during non-peak hours with lower prices. Based on different values of the α parameter in each hour, the sensitivity of load shifting is different that will have impact on the trade-off potentials. At the end, the expected value of perfect information (EVPI) is also calculated for TOU ($\theta = 20$) by subtracting the DSO objective value of the stochastic model from the mean DSO objective value of 20 single scenarios, which is about \$7244 representing the cost the DSO is willing to pay for perfect prediction on the uncertain parameters.

4. THE ROBUST HIERARCHICAL MODEL-FREE TRANSACTIONAL CONTROL APPROACH

In this section, a bilevel electricity pricing and demand response Stackelberg game between the DSO and LAs is considered, and a robust decision model is proposed for the DSO to deal with the uncertainties from the wholesale market prices and demand consumptions of LAs. In the upper level, the objective of the DSO is in max-min form to maximize the minimum payoff, while the LAs at the lower level maximize their own utility values. With the max-min objective at the upper level, the robust bilevel model is converted into a single level model by the Karush-Kuhn-Tucker (KKT) conditions and prime-dual transformation. The building level temperature preference is guaranteed by the virtual battery constraints in the model derived from the building thermal properties. Several groups of case studies have been conducted based on different preferences on uncertainty gaps and peak load reductions to show its effectiveness. After-the-fact scenario analysis has indicated that the robust solution is more beneficial in reducing the risk of inaccurate predictions as compared to the risk neutral strategy.

4.1 PRICING-DEMAND RESPONSE

In this section, we review the proposed DR pricing game in Section 2, with slight change to the notations to better fit the robust game introduced in Section 4.2. All the parameters and variables are listed in Table VI, followed by the mathematical model.

Table VI. Notations for the robust game model.

Indices	
T, t, n	Total hours, index for hours, LAs
Parameters	
$C_t, \overline{P}$	Marginal cost, price upper bound
$\underline{H}_{n,t}, \overline{H}_{n,t}$	Lower & upper bound of thermal demand
$\underline{L}_{n,t}, \overline{L}_{n,t}$	Lower & upper bound of non-thermal demand
$Dh_{n,t}, Dd_{n,t}$	Nominal thermal, non-thermal demand
$\alpha_{n,t}, \theta$	Satisfaction preferences of LAs, penalty coef.
BI, ϵ	Initial level, Dissipation rate of virtual battery
$\underline{B}_{n,t}, \overline{B}_{n,t}$	Lower bound, upper bound for virtual battery
Variables	
$p_t, dl_{n,t}$	Electricity price, total electricity load
$hr_{n,t}, dr_{n,t}$	Resulted thermal load, non-thermal load
$m, b_{n,t}$	Peak load, storage level in virtual battery

In the investigated DR game here, the DSO is the leader that makes decisions on the electricity price by considering the demand responses from the LAs, which are followers in the lower level. The objective of

the DSO is to maximize its overall utility, which includes its profit (first two terms in (35)), peak load penalty (fourth term in (35)), and the overall customer satisfaction (third term in (35)) that represents its social obligation.

$$DSO: \quad \max U_o = \sum_{n,t} p_t \cdot dl_{n,t} - \sum_{n,t} C_t \cdot dl_{n,t} + \sum_{n,t} S\,(Dl, dl) - \theta \cdot T \cdot m \tag{35}$$

$$C_t \le p_t \le \overline{P},\ \forall t \tag{36}$$

$$m \ge \sum_{n} d\,l_{n,t},\ \forall t \tag{37}$$

The constraints for the DSO optimization are the price range in (36) and the peak load calculation in (37).

At the lower level, each LA also tries to maximize its own utility, which consists of its consumption satisfaction and the electricity bill payment in (38). The resulted load profile is the summation of the thermal load hr and the non-thermal load dr in (39). Equation (40) defines the range for the non-thermal load in each time step, and (41) defines its overall shifting flexibility for the considered decision period. Equation (42) defines the range for thermal load. The virtual battery constraints in (43)-(45) are derived based on the building thermal characteristics and are used to guarantee a pre-defined temperature band of each aggregated building. The difference between the actual power consumed hr by a thermal appliance and its nominal thermal load Dh determines whether the virtual battery is being charged or discharged. ϵ is the virtual battery dissipation rate, which depends on the properties of the thermal load (e.g., insulation characteristics) and can be determined empirically. Equation (46) ensures that the virtual battery level at the end of the day equals to its initial level.

$$LAs: \max U_n = \sum_{t} S\,(Dl, dl) - \sum_{t} p_t \cdot dl_{n,t} \tag{38}$$

$$dl_{n,t} = hr_{n,t} + dr_{n,t}:\ \lambda_{n,t}^{c3} \tag{39}$$

$$\underline{L}_{n,t} \le dr_{n,t} \le \overline{L}_{n,t}:\ \underline{\lambda}_{n,t}^{c4}, \overline{\lambda}_{n,t}^{c4} \tag{40}$$

$$0.9 \cdot \sum_{t} D\,d_{n,t} \le \sum_{t} d\,r_{n,t} \le 1.1 \cdot \sum_{t} D\,d_{n,t}:\ \underline{\lambda}_{n,t}^{c5}, \overline{\lambda}_{n,t}^{c5} \tag{41}$$

$$\underline{H}_{n,t} \le hr_{n,t} \le \overline{H}_{n,t}:\ \underline{\lambda}_{n,t}^{c6}, \overline{\lambda}_{n,t}^{c6} \tag{42}$$

$$\underline{B}_{n,t} \le b_{n,t} \le \overline{B}_{n,t}:\ \underline{\lambda}_{n,t}^{c7}, \overline{\lambda}_{n,t}^{c7} \tag{43}$$

$$b_{n,t} = \epsilon \cdot (BI_n + hr_{n,t} - Dh_{n,t}):\ \lambda_{n,t=1}^{c8} \tag{44}$$

$$b_{n,t} = \epsilon \cdot (b_{n,t-1} + hr_{n,t} - Dh_{n,t}):\ \lambda_{n,t\ge 2}^{c8} \tag{45}$$

$$b_{n,t=T} = BI_n:\ \lambda_{n}^{c9} \tag{46}$$

The consumption satisfaction function $S(Dl, dl)$ is defined as $S(Dl, dl) = Dl_{n,t} \cdot w_{n,t} \cdot f(\frac{dl_{n,t}}{Dl_{n,t}})$. Note that $Dl_{n,t} = Dh_{n,t} + Dd_{n,t}$ is the total nominal load; w is a user defined parameter; and α represents the sensitivity of demand shifting. To reduce the computational burden and guarantee optimality, the satisfaction function S is linearized into two linear segments at the intersection point x_0 where $f'(x_0) = 1$, thus $x_0 = (\frac{1}{\alpha})^{\frac{1}{\alpha-1}}$. Since α is also a step dependent parameter, x_0 is different for each time step. Hence, the first linear segment passes through the two points (0, 0) and (x_0, x_0^{α}), and the second linear segment goes through the two points (x_0, x_0^{α}) and (1, 1). Thus, the following two satisfaction function constraints need to be added to the lower-level model. The lower-level model for LAs in the DR game becomes (38)-(48), where the dual variable of each constraint is presented following a colon.

$$S_{n,t} \leq w_{n,t} \cdot x_0^{\alpha_{n,t}-1} \cdot dl_{n,t} : \lambda_{n,t}^{c1} \tag{47}$$

$$S_{n,t} \leq w_{n,t} \cdot dl_{n,t} \cdot \frac{1 - x_0^{\alpha_{n,t}}}{1 - x_0} + w_{n,t} \cdot Dl_{n,t} \cdot \frac{x_0^{\alpha_{n,t}} - x_0}{1 - x_0} : \lambda_{n,t}^{c2} \tag{48}$$

The developed bilevel model in this section is a deterministic model, which corresponds to the risk-neural strategy for the DSO. In the next subsection, a robust bilevel optimization model is derived based on this deterministic model to cope with the parameter uncertainties.

4.2 ROBUST OPTIMIZATION MODEL

4.2.1 BILEVEL MODEL

In this section, the robust decision is made from the perspective of the DSO. To consider the related risk of the forecasted parameters $\tilde{C}_t, \widetilde{Dh}_{n,t}, \widetilde{Dd}_{n,t}$, a new variable set $\Delta = \{\Delta C_t, \Delta Dh_{n,t}, \Delta Dd_{n,t}\}$ is introduced to represent the deviation of the forecasted parameters. The robust factors $\gamma_c, \gamma_h, \gamma_d$ are defined by the decision makers to evaluate the length of the uncertain gap around the forecasted parameters. Since robust optimization stands at the risk-averse view point, the worst case of uncertainties occurrence in the allowable uncertain range is evaluated [66]. The robust bilevel optimization model is formulated as:

$$DSO: \max_{p,dl} \quad \min_{\Delta} U_o = \sum_{n,t} p_t \cdot dl_{n,t} - \sum_{n,t} (\tilde{C}_t + \Delta C_t) \cdot dl_{n,t} + \sum_{n,t} S(\widetilde{Dl}, dl) - \theta \cdot T \cdot m \tag{49}$$

$$\tilde{C}_t + \Delta C_t \leq p_t \leq \overline{P}, \ \forall t \tag{50}$$

$$m \geq \sum_{n} d\, l_{n,t}, \ \forall t \tag{51}$$

$$-\gamma_c \cdot \tilde{C}_t \leq \Delta C_t \leq \gamma_c \cdot \tilde{C}_t, \ \forall t \tag{52}$$

$$-\gamma_h \cdot \widetilde{Dh}_{n,t} \leq \Delta Dh_{n,t} \leq \gamma_h \cdot \widetilde{Dh}_{n,t}, \ \forall n, t \tag{53}$$

$$-\gamma_d \cdot \widetilde{Dd}_{n,t} \leq \Delta Dd_{n,t} \leq \gamma_d \cdot \widetilde{Dd}_{n,t}, \ \forall n, t \tag{54}$$

As observed in the robust model for the DSO, its objective is maximized with respect to its main decision variables p, dl and minimized by the uncertain parameter set Δ. The length of the uncertain gap can be adjusted by the robust factors.

Similarly, the constraints (41), (44), (45), and (48) in the lower-level model are updated as:

$$0.9 \cdot \sum_t (\widetilde{Dd}_{n,t} + \Delta Dd_{n,t}) \leq \sum_t d\, r_{n,t} \leq 1.1 \cdot \sum_t (\widetilde{Dd}_{n,t} + \Delta Dd_{n,t}) \tag{55}$$

$$b_{n,t} = \epsilon \cdot (BI_n + hr_{n,t} - \widetilde{Dh}_{n,t} - \Delta Dh_{n,t}) \tag{56}$$

$$b_{n,t} = \epsilon \cdot (b_{n,t-1} + hr_{n,t} - \widetilde{Dh}_{n,t} - \Delta Dh_{n,t}) \tag{57}$$

$$S_{n,t} \quad \leq w_{n,t} \cdot dl_{n,t} \cdot \frac{1 - x_0^{\alpha_{n,t}}}{1 - x_0} + w_{n,t} \cdot (Dl_{n,t} + \Delta Dh_{n,t} + \Delta Dd_{n,t}) \cdot \frac{x_0^{\alpha_{n,t}} - x_0}{1 - x_0} \tag{58}$$

The resulted robust bilevel model now becomes the upper-level model (49)-(54) and the lower-level model (38)-(40), (42)-(43), (46)-(47), and (55)-(58).

4.2.2 SINGLE-LEVEL MODEL

To be able to solve the problem with commercial solvers, the equivalent single level optimization model needs to be obtained. The process to transform the proposed bilevel robust model into a single level model has two main steps: KKT transformation and prime-dual transformation.

In KKT transformation, since the variables in the upper level are treated as parameters in the lower-level model of LAs that is then linear and convex, it can be substituted into the upper-level model by its equivalent KKT optimality conditions. This process has been conducted in related works frequently [67, 68], for the sake of conciseness, we avoid repeating it here. In this transformation, the strong duality theorem in (59)-(61) is used to replace the bilinear term $p_t \cdot dl_{n,t}$ in objective (49). Assume Λ is the prime variables set in the lower model of LA, then

$$\sum_t S_{n,t} - \sum_t p_t \cdot dl_{n,t} = G(\Lambda) + G(\Delta) \tag{59}$$

$$\begin{aligned} G(\Lambda) = \sum_t [\, & w_{n,t} \cdot (\widetilde{Dh}_{n,t} + \widetilde{Dd}_{n,t}) \cdot \frac{x_0^{\alpha} - x_0}{1 - x_0} \cdot \lambda_{n,t}^{c2} - \\ & \underline{L}_{n,t} \cdot \underline{\lambda}_{n,t}^{c4} + \overline{L}_{n,t} \cdot \overline{\lambda}_{n,t}^{c4} - H_{n,t} \cdot \lambda_{n,t}^{c6} + \overline{H}_{n,t} \cdot \overline{\lambda}_{n,t}^{c6} - \\ & \underline{B}_{n,t} \cdot \underline{\lambda}_{n,t}^{c7} + \overline{B}_{n,t} \cdot \overline{\lambda}_{n,t}^{c7}] - \sum_t 0.9 \cdot \underline{\lambda}_n^{c5} \cdot \widetilde{Dd}_{n,t} + \\ & \sum_t 1.1 \cdot \overline{\lambda}_n^{c5} \cdot \widetilde{Dd}_{n,t} - \sum_t \epsilon \cdot \lambda_{n,t}^{c8} \cdot \widetilde{Dh}_{n,t} + \\ & \epsilon \cdot BI_n \cdot \lambda_{n,t=1}^{c8} + BI_n \cdot \lambda_n^{c9} \end{aligned} \tag{60}$$

$$G(\Delta) = \sum_t [\, w_{n,t} \cdot (\Delta Dh_{n,t} + \Delta Dd_{n,t}) \cdot \frac{x_0^{\alpha} - x_0}{1 - x_0} \cdot \lambda_{n,t}^{c2} - \sum_t 0.9 \cdot \underline{\lambda}_n^{c5} \cdot \Delta Dd_{n,t} + \sum_t 1.1 \cdot \overline{\lambda}_n^{c5} \cdot \Delta Dd_{n,t} - \sum_t \epsilon \cdot \lambda_{n,t}^{c8} \cdot \Delta Dh_{n,t} \tag{61}$$

After the KKT transformation and $p_t \cdot dl_{n,t}$ replacement in the upper level, the robust bilevel model becomes a single level max-min optimization. Since the minimization in (49) is with respect to Δ, the objective of the final single level optimization can be rewritten as in (62)-(64). Together with other related constraints, the final single level max-min model is given as:

$$DSO\text{: max } z \tag{62}$$

$$2 \cdot \sum_{n,t} S_{n,t} - \sum_n G\,(\Lambda) - \sum_{n,t} \tilde{C}_t \cdot dl_{n,t} - \theta \cdot T \cdot m - \min_{\Delta}\{\sum_n G\,(\Delta) - \sum_{n,t} \Delta\, C_t \cdot dl_{n,t}\} \geq z \tag{63}$$

(50)-(58), (39)-(40), (42)-(43), (46)-(47), KKT conditions of the lower level (64)

In order to unify the problem as a final max optimization, the duality theorem is used to convert the inside min optimization to a max optimization by replacing the original min optimization with its max dual optimization problem. The method is well described in [66, 69]. After applying the above transformation, the final single level mixed integer programming model is obtained. The commercial solver CPLEX is used to solve the final model.

4.3 NUMERICAL CASE STUDY

In this section, the developed robust bilevel optimization is demonstrated by several groups of experiments. Five LAs are considered in the case study, and the nominal thermal load Dh of each LA consists of 1000 residential & commercial HVACs and water heaters, see Figure 18. So, in total there are 5000 TCLs considered in this study. The detailed process to generate the data refers to [38, 39]. The nominal non-thermal load Dd in Figure 19 is adopted from [70] and mixed based on a commercial building reference load. The marginal cost C_t is the same as in [52]. $\alpha_{n,t}$ is assumed the same for all LAs as shown in Figure 20.

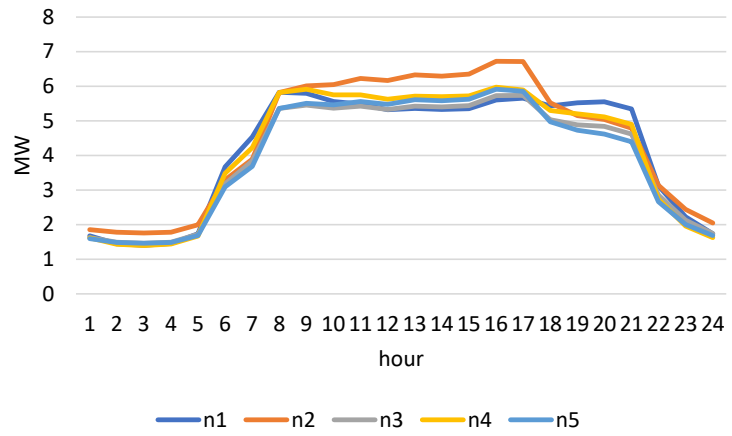

Figure 18. Nominal thermal load of LAs (n refers to LA).

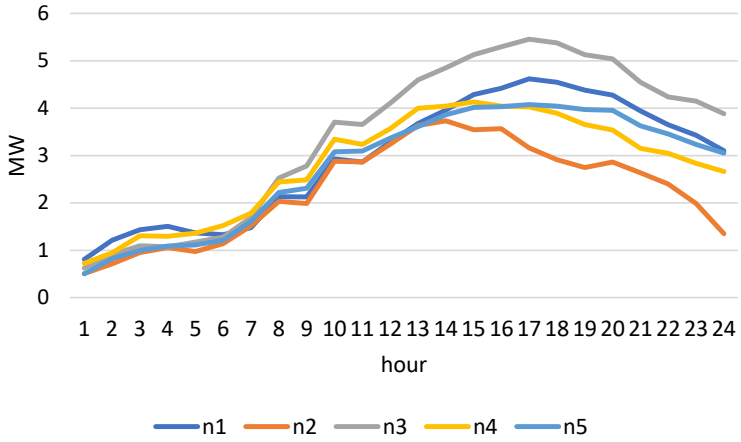

Figure 19. Nominal non-thermal load of LAs (n refers to LA).

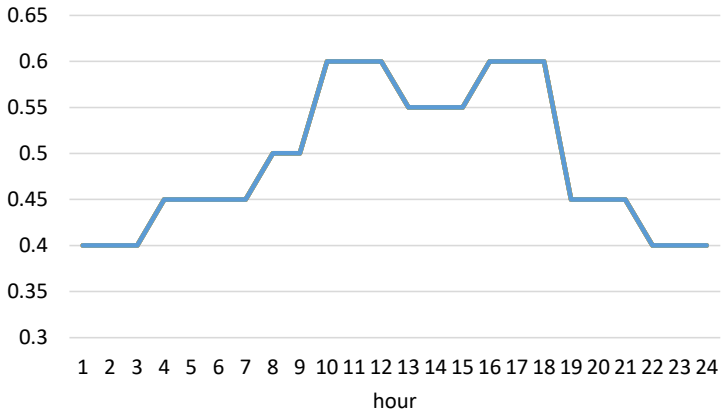

Figure 20. α preference in satisfaction function.

Based on the different robust gap length settings γ $(= \gamma_c = \gamma_d = \gamma_h)$ on the uncertainties in (52)-(54) and the peak load penalty θ in (49), the objective value of the DSO and the resulted peak load from the robust bilevel optimization are illustrated in Figure 21. As observed, the DSO objective decreases when the penalty θ increases with the same gap level; this is because the overall satisfaction term and penalty term in the objective function both move against maximization. Furthermore, the DSO objective also drops when the robust gap length increases from 0 to $\pm$ 20%; this is because the robust optimization targets the worst-case scenario in the uncertainty range. The peak load has a similar trend, and it is stabilized with max γ despite of the different θ levels due to the flexibility limitation of the load profile.

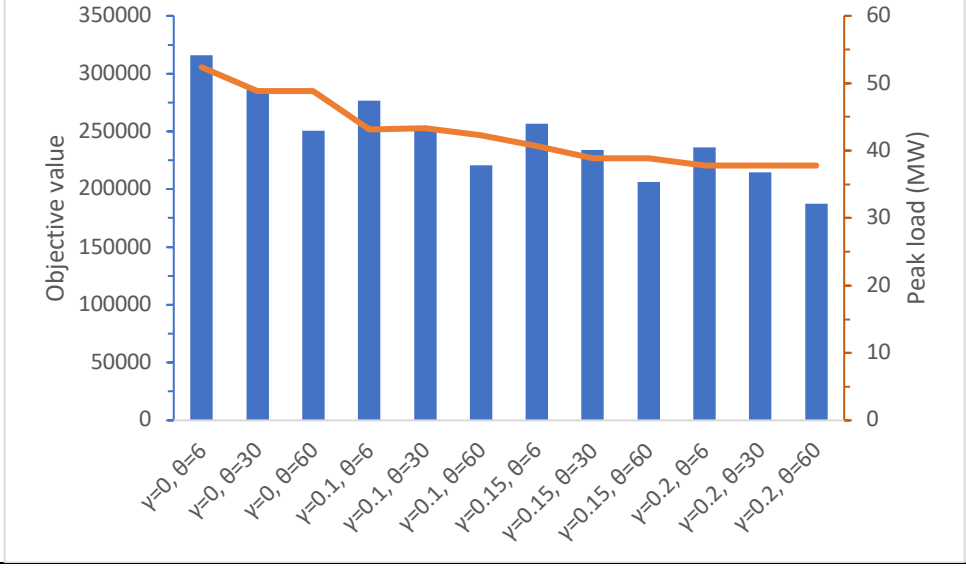

Figure 21. DSO objective and peak load of the robust optimization under different cases.

Take the peak penalty $\theta = 60$ as an example, the resulted electricity prices and load profiles under different uncertainty gap lengths are shown in Figures 22 and 23. To optimize against more uncertainties from the wholesale marginal cost and customers' overall consumption, the DSO tends to increase the prices until the allowable upper bound, especially in the high load range hour 8-21, see the nominal load profile in Figure 23. The load shifting from peak hours to off-peak hours and peak load reduction can also be observed in Figure 23.

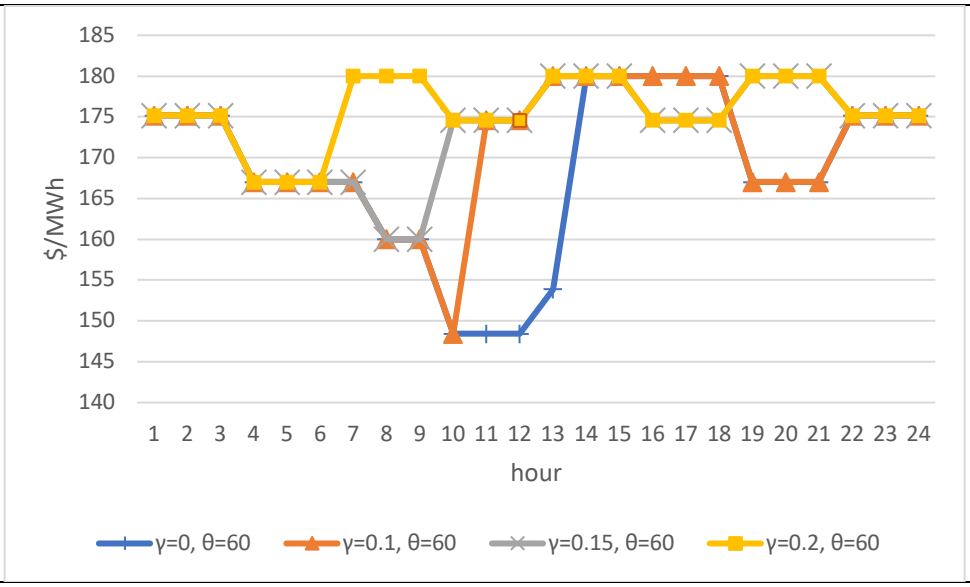

Figure 22. Price signals of the robust optimization under different cases.

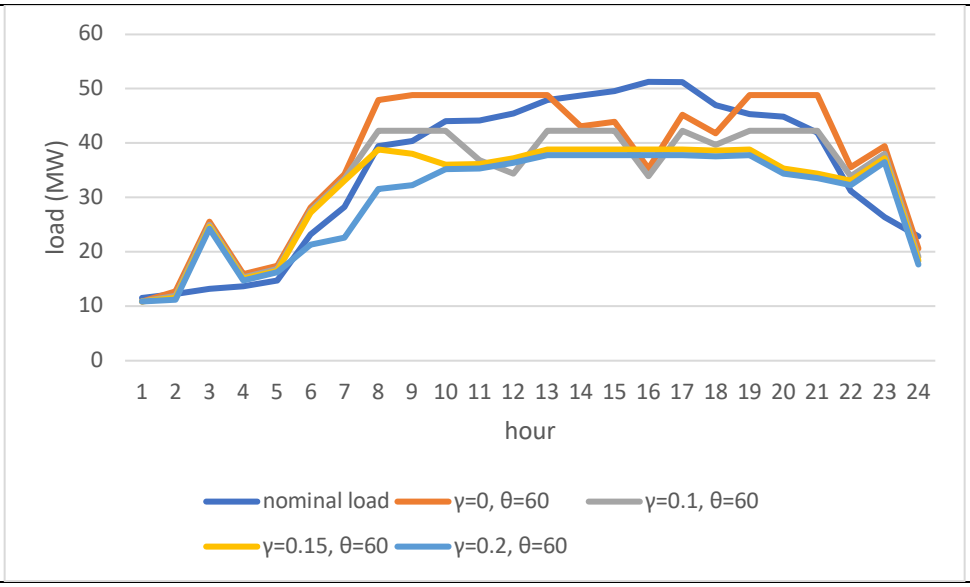

Figure 23. Resulted load profiles of the robust optimization under different cases.

With the results of the robust models in several cases, MFC is used to allocate the optimal aggregate load profiles among the various TCLs under each LA. Figures 24-27 show the temperature responses of the thermal loads for one LA (325 residential HVAC units, 336 commercial HVAC units, 339 water heater units). As observed, the MFC strategy was able to maintain temperatures within the comfort bounds at all times.

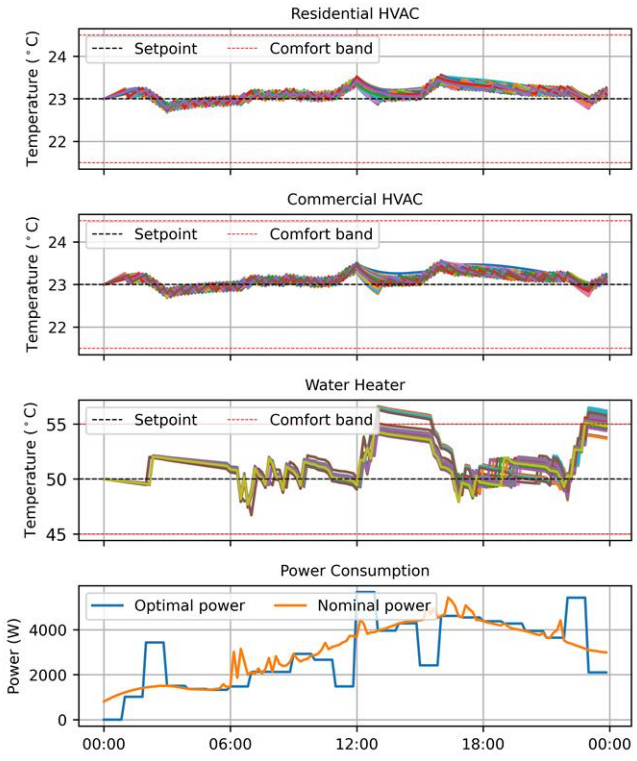

Figure 24. Temperature responses and power tracking of TCLs ($\gamma = 0, \theta = 60$).

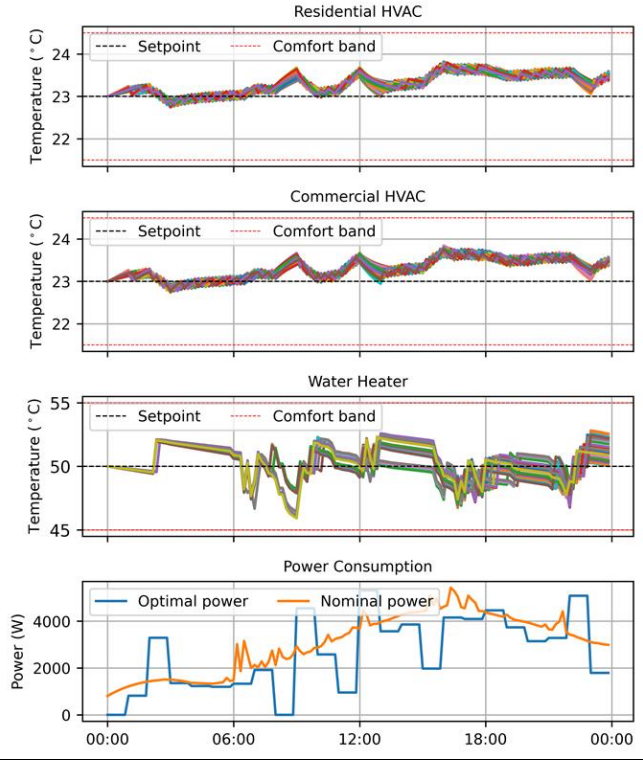

Figure 25. Temperature responses and power tracking of TCLs ($\gamma = 0.1, \theta = 60$).

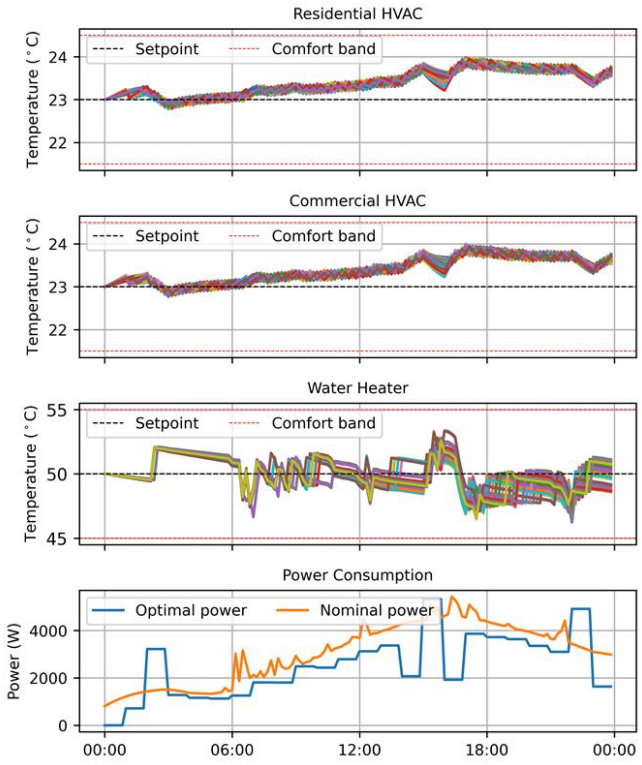

Figure 26. Temperature responses and power tracking of TCLs ($\gamma = 0.15, \theta = 60$).

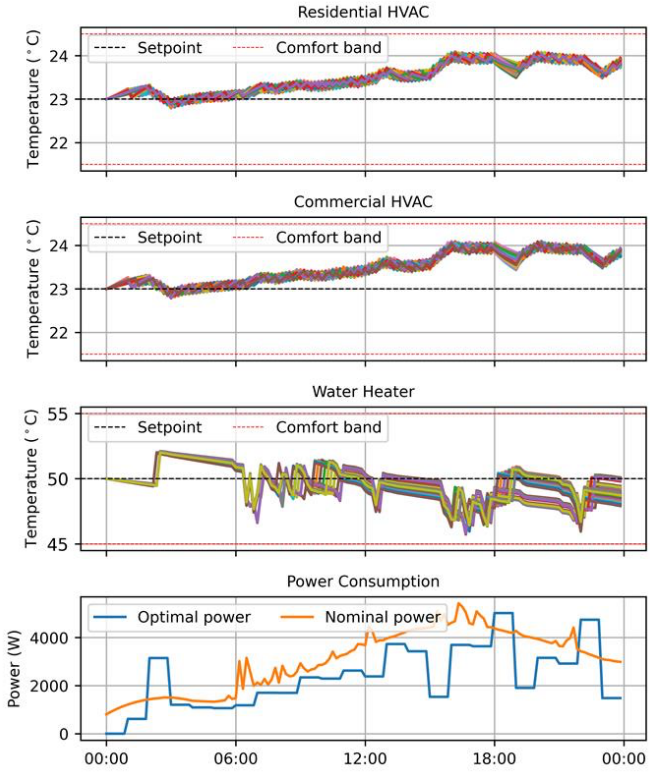

Figure 27. Temperature responses and power tracking of TCLs ($\gamma = 0.2, \theta = 60$).

To illustrate the impact of considering uncertainty in the studied problem, after-the-fact analysis is conducted to compare the risk neutral strategy and the proposed robust strategy. After-the-fact scenarios are generated by adding $\pm$ 20% random noise to the three considered uncertainty parameters $C_t, Dh_{n,t}, Dd_{n,t}$. Two hundred scenarios are generated for this analysis. In Figure 28, the DSO objective from the robust bilevel model is \$187375.2, which is the guaranteed lower bound with uncertainty gap $\pm$ 20%. While the objective value from the neutral model without uncertainty ($\gamma = 0$ assume prediction is accurate) is \$250716.5. However, after the resulted price decisions from the robust and neutral models are fixed and used to solve the lower-level models (in (38)-(46)) over the 200 scenarios, the expected DSO objective value of robust price strategy (\$262568.2) is higher than that of neutral price strategy (\$256104.6). These results show the effectiveness of the proposed robust decision approach and thus indicate the importance of modeling uncertainties.

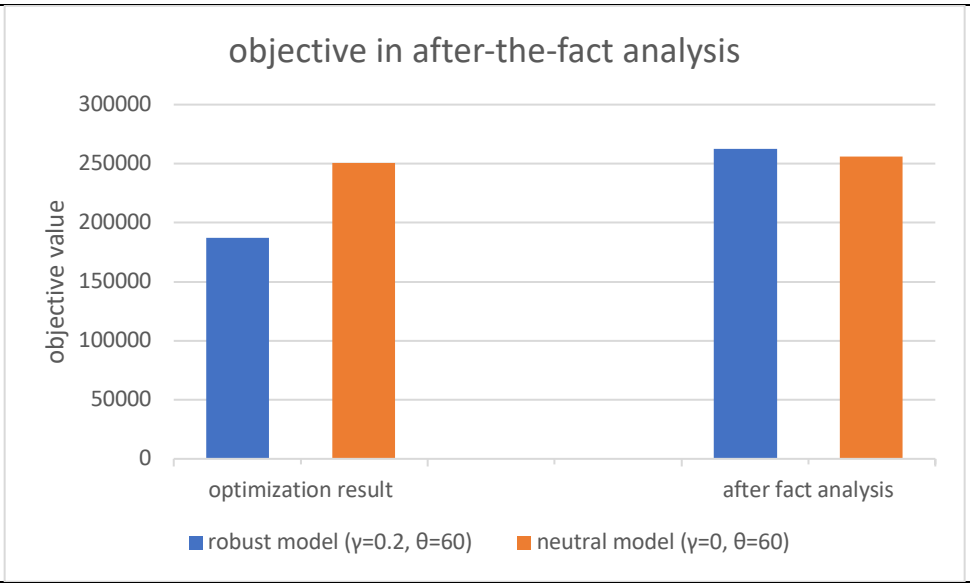

Figure 28. The DSO objectives of robust and neutral strategies in after-the-fact analysis.

The total energy consumption for the deterministic (developed in Section 2), stochastic (developed in Section 3), and robust (developed in this section) transactive optimization strategies for one day is shown in Table VII. It is observed that the robust optimization approach consumes the lowest energy, since it addresses the worst-case (lower-bound) scenario. Also, it is observed that the proposed TOU pricing scheme does not consume more energy than the (optimized) fixed pricing scheme as in most conventional transactive schemes; indeed, it consumes a bit less energy.

Table VII. A comparison of 24-hour energy consumption (in MW) for 10 LAs (10,000 TCLs) using various optimization strategies and pricing schemes ($\theta = 10, \gamma = 10$).

	Deterministic	Stochastic	Robust
Fixed Pricing	1716	1702	1618
TOU Pricing	1712	1693	1600

In summary, the electricity pricing problem of a DSO is presented in this section with the consideration of DR from LAs and modeled as a bilevel problem. The uncertainties on LAs' energy consumption and the electricity marginal cost are dealt with using a robust optimization with the attitude of risk averse. Based on the KKT optimality conditions, the lower-level model is substituted into the upper-level model, and dual transformation is used to convert the nested max-min objective of the DSO into a single level maximization form. The experimental results have shown that the DSO tends to raise the price when the risk of demand

uncertainty is higher. Moreover, the robustness of the price strategy from the proposed robust bilevel model is tested against random after-the-fact scenarios and compared to the risk-neutral model. Although the risk-neutral strategy has higher objective value than the robust optimization (worse case), the robust strategy has higher expected objective value than the risk-neutral strategy by taking the actual prediction errors into account, and thus it is more immune to the related risk of predictions.

5. FIELD TESTING AND VALIDATION OF THE HIERARCHICAL MODEL-FREE TRANSACTIONAL CONTROL APPROACH

This section presents a field implementation and testing of the hierarchical model-free transactive control strategy using residential building TCLs in real-world setting. Two different sites are selected for the testing: "Yarnell Station" residential house located in Knoxville, Tennessee, and "Altus at The Quarter" smart neighborhood in Atlanta, Georgia. The achieved experimental field-testing results demonstrate the effectiveness of the proposed transactive control strategy.

5.1 FIELD TESTING AT YARNELL STATION RESIDENTIAL HOUSE

The house used for the field testing is a single-family two-story building (2400 sqft) in an area located in Knoxville, Tennessee, USA (see Figure 29). It is a research house with emulated occupancy, and it is equipped with two single-zone HVAC units and one 66-gallon electric WH. This test is conducted for one month in the winter of 2021 to test the proposed transactive control strategy with a variety of conditions and scenarios. To scale up the testing, we added eight simulated single-zone HVAC units (only HVACs are considered in this test). So, the experiment included 10 HVAC units in total, 2 actual and 8 simulated.

Figure 29. Yarnell Station residential house used in the field testing.

The framework of the fully automated approach is shown in Figure 30, where day-ahead weather data is retrieved from a publicly available weather API (i.e., OpenWeather API [71]). Then, using the day ahead weather data, the aggregate virtual battery model computes the feasibility constraints and passes them to the optimization engine. In the optimization engine, the price and power profiles are hourly optimized using the bilevel Stackelberg game, and the optimal power is passed to the control engine. In the control engine, MFC controls the actual TCL units every 15 minutes through Ecobee and Skycentrics APIs (shown in brown solid arrow (control setpoint signals) and blue solid arrows (received measurements)), while MFC controls the simulated units directly (shown in black solid arrows (control signals and received temperature measurements)). When controlling the TCL units, MFC has two objectives. First, MFC ensures that the temperature responses are within the comfort bands. Second, the optimal power profile provided by the optimization engine is being tracked by the total power consumption of the TCLs.

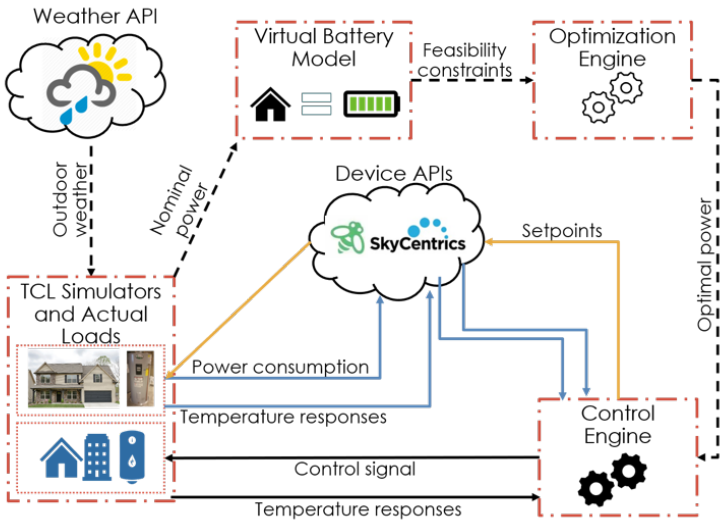

Figure 30. The framework of the fully automated field testing.

Figures 31-33 show the performance of the fully automated approach in three randomly selected days (the temperature responses of the two actual HVACs are shown in dashed lines in the top plots). Although the weather forecasts are accurate for most of the time, there were other times the actual weather was slightly different from the forecasted one. Despite that, the proposed approach was able to achieve all three intended objectives. First, the MFC controllers were able to maintain the temperatures within the comfort band. Second, the virtual battery-integrated game theory was able to reduce the peak load. Third, the MFC controllers were able to track the optimal power profile resulted from the virtual battery-integrated game theory optimization.

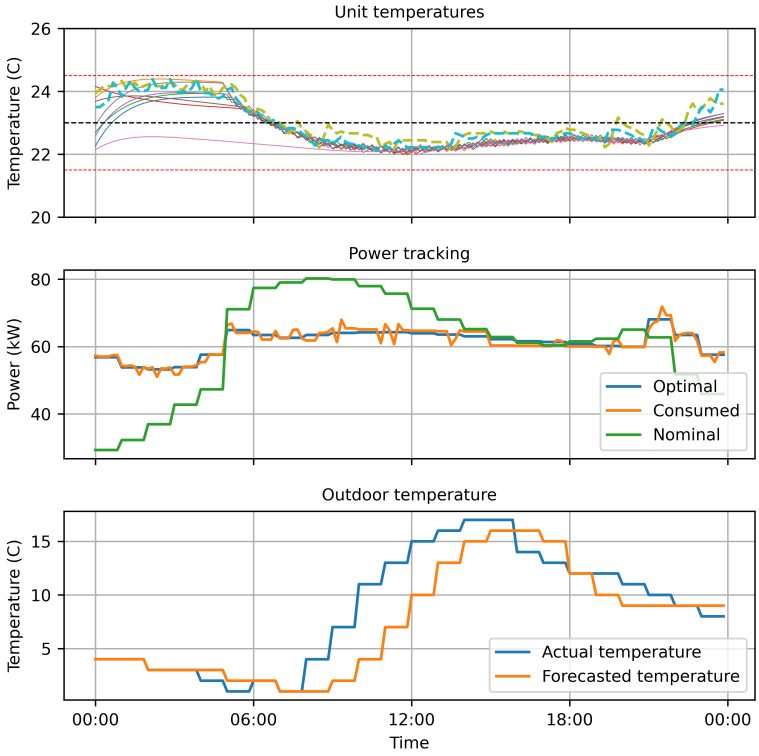

Figure 31. Field testing results for Day 1.

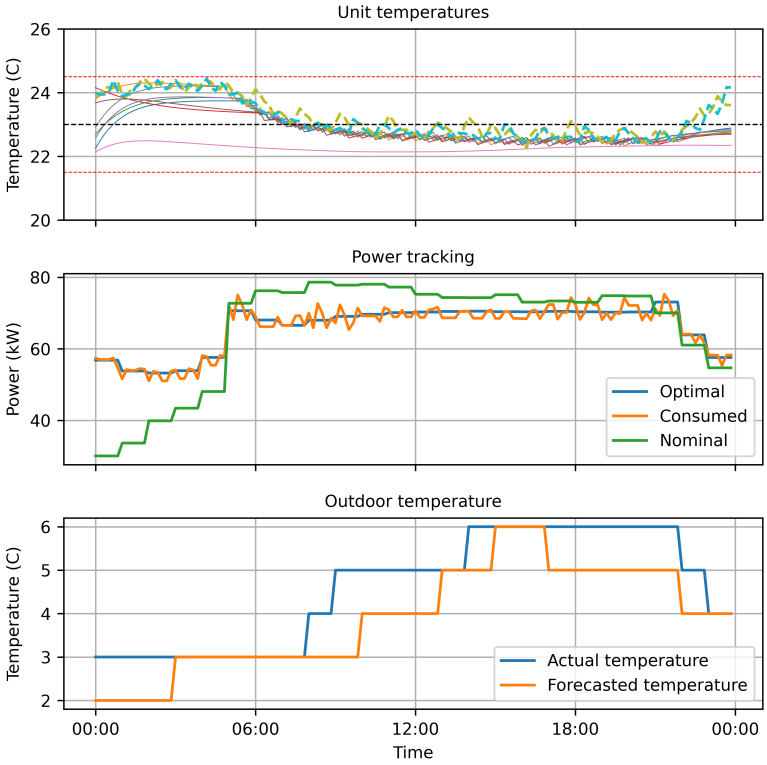

Figure 32. Field testing results for Day 2.

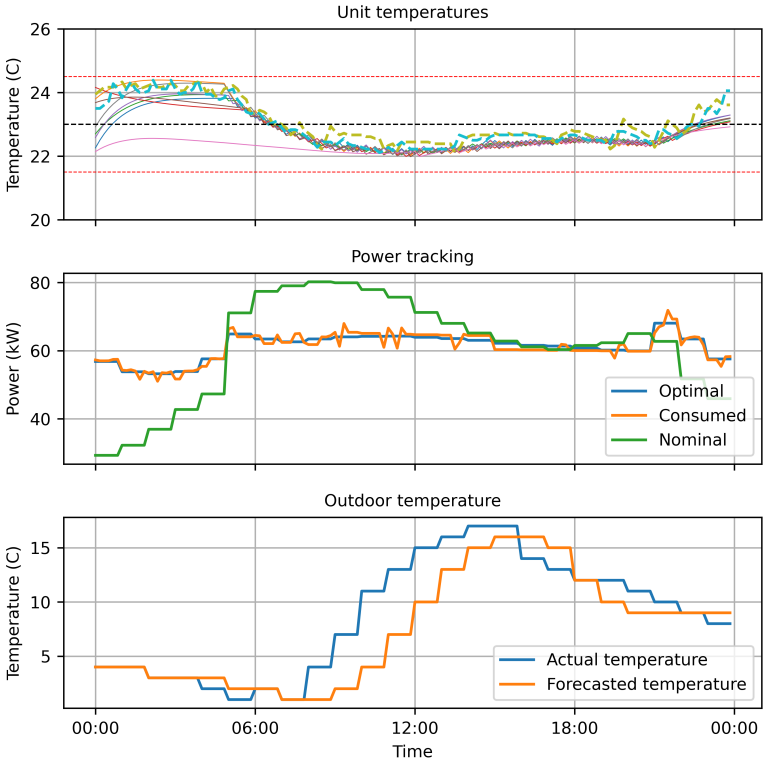

Figure 33. Field testing results for Day 3.

5.2 FIELD TESTING AT ALTUS SMART NEIGHBORHOOD

The test site for the field testing is a residential neighborhood in Atlanta, Georgia constructed by the Southern Company (see Figure 34). These homes are occupied and therefore demonstrate the behavior of actual inhabited homes. The homes themselves are four stories, with each story (referred to as zone moving forward) having its own thermostat. The fourth zone has a separate Lennox Mini-Split for cooling, while the three other zones share an HVAC unit, with their individual thermostats coordinate via a zone control board. Due to the lack of a reliable communication, the fourth floor was not utilized by the control in this field test. The control algorithm was tested for two weeks in summer of 2021. The experiment included a total of five GEBs, with the choice of homes approved by Southern Company. The control was implemented on a VOLTTRON software platform [72] using an agent-based approach. In these experiments, an API developed by Southern Company was utilized to implement the proposed transactive control approach.

Figure 34. "Altus at The Quarter" smart neighborhood used in the field testing.

Each relevant appliance is "smart" and networked to a vendor API (i.e., Ecobee) over site Wi-Fi. Southern Company has provided an intermediate API that anonymizes and serves the data to the research team. Southern Company parsing all data in front of the Oak Ridge National Laboratory (ORNL) team serves to both ensure ORNL team never has access to identifying information and keep any customer-facing interactions (such as device support) to Southern Company. Figure 35 shows the neighborhood data flow. To keep with cyber security requirements and ensure a safe and reliable deployment, the controller is hosted by Ace IoT [73]. They also provide some data recording services.

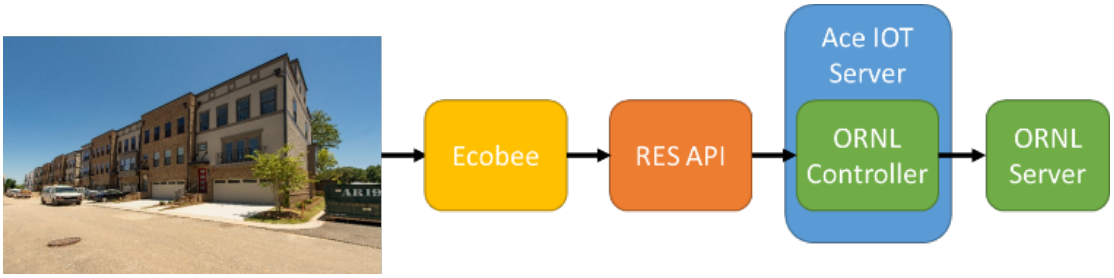

Figure 35. Neighborhood data flow.

The controller is an agent-based system with agents responsible for data gathering, MFC control, and aggregated optimization. One key benefit of utilizing VOLTTRON is the potential for securely scaling deployments across a wide geographic area. While the physical implementation of this test does not reach such scale, the architecture has been constructed in a way that the application can be scaled to many LAs coordinated through the optimization. In this case, all agents are run on a single VOLTTRON instance. Scaling up this architecture would only require introducing new MFC Agents and ensuring secure multiplatform communication.

Figure 36 shows the physically co-located architecture. There are two hierarchies of responsibility: the game-theoretic utility control of the LA and the device level control within the LA. At the start of every control run, the LA, represented by the MFC agents, publishes LA-specific estimated power consumption information to the Game Theoretic Control Agent. This agent computes an optimization to tailor specific consumption profiles for the LA and then sends the profile downwards. The MFC agents are responsible for steering their respective devices along the prescribed trajectory. This control flow can be halted and restarted depending on the control timelines. Figure 37 shows the control flow, where the blue color represents an action by the game theoretic controller, and the orange color represents actions by the MFC controllers.

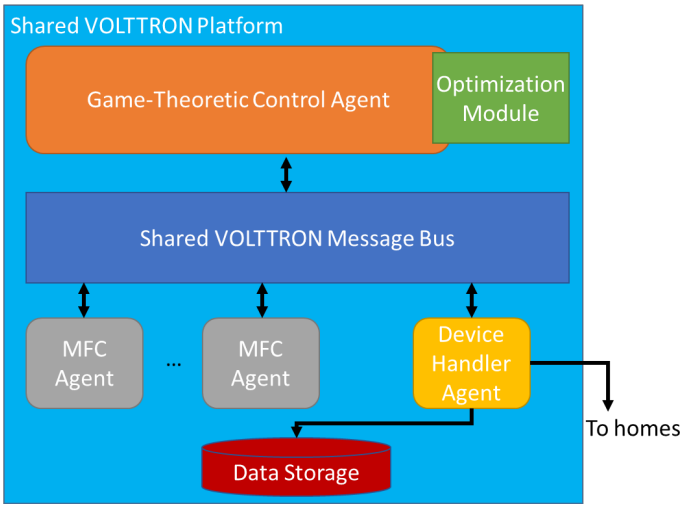

Figure 36. Physically co-located VOLTTRON architecture.

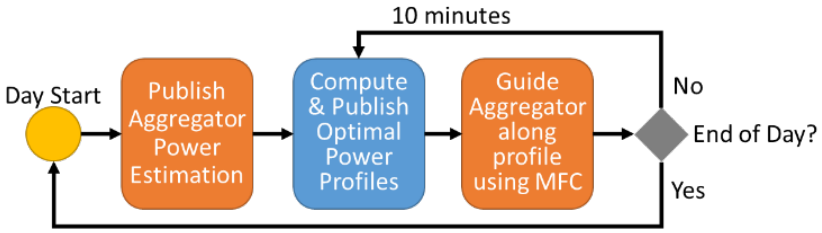

Figure 37. Control flow.

The control system uses the VOLTTRON software platform and as such is a Python program. Because there is a non-linear optimization component, the open-source solver IPOPT [74] is utilized for the game-theoretic optimization. The database underlying the system is a time-series database called InfluxDB [75]. Upon maturity, the system can be containerized and deployed to a cloud architecture using Docker [76] that is accessible for any urgent patching. Grafana [77] is used to monitor the results and data collection coming out of the controller.

The homes that are controlled at the Southern Company test site are fully occupied homes, with access granted to the ORNL controller through the Southern Company contract with the homeowners. As such, much care is taken to err on the conservative side of control. That is, as much as possible, the control must steer the control signal within a relatively narrow band around the preferred customer setpoint. In the case of this field test, temperatures were allowed to stray 0.5°C above the recorded preferred temperature, and 1°C below the preferred temperature, resulting in a 1.5°C band that the control can operate within. Further, homeowner interventions (termed "overrides") must be adhered to, with the control adjusted to potentially unforeseen setpoints.

Several pieces of data are necessary in order to build the power forecast for the LA and then optimize for a power profile. The two main external pressures on the system are the temperature forecast and the solar forecast. These are gathered in two different ways: (1) The temperature forecast is taken from the OpenWeather API [71]. This is an API with a free tier that allows for hourly forecasting. (2) The solar forecast is a resource provided by Southern Company. An hourly forecast is given for 12 hours from the current hour. If a longer than twelve-hour forecast is needed, the solar forecast is inverted and appended to the end. The values provided by the solar forecast are Global Horizontal Irradiance (GHI), Diffuse Horizontal Irradiance (DHI), and Direct Normal Irradiance (DNI). The temperature and solar forecasts were used in conjunction with a data-driven model of the test site homes, with parameters trained using two weeks of historical data. This model is used to construct a forecast of the nominal power consumption of the individual homes for the incoming control window.

Figures 38-40 show the performance of the proposed two-layer transactive controller approach on sample three days for the selected buildings of the Southern Company Smart Neighborhood Facility. The proposed control approach was able to mostly achieve all intended objectives. First, the MFC controllers were always able to maintain the temperatures within the comfort band. Nevertheless, the building occupants were always allowed to override the temperature setpoints set by our controller by simply adjusting their thermostats. Second, the virtual battery-integrated game theory was able to reduce the peak load. Figures 38-40 clearly show that the optimal power profile has lower peak than the nominal power profile. Third, the MFC controllers were mainly able to track the optimal power profile resulted from the virtual battery-integrated game theory optimization. For example, on June 23, the tracking performance of MFC was perfect except for a few exceptions. However, on June 22, the tracking performance was relatively poorer. The tracking performance is affected by many factors including communication issues, occupant overrides, unexpected weather patterns, and thermostat API and server failures. In particular, on June 23 at 15:41, we lost connection to the thermostats and failed to track optimal power around that time, which resulted in a peak power consumption. Similarly, on June 22 we experienced several communication issues, and observed that occupants overrode the setpoints set by our controller. For this reason, the tracking performance on June 22 was relatively poorer.

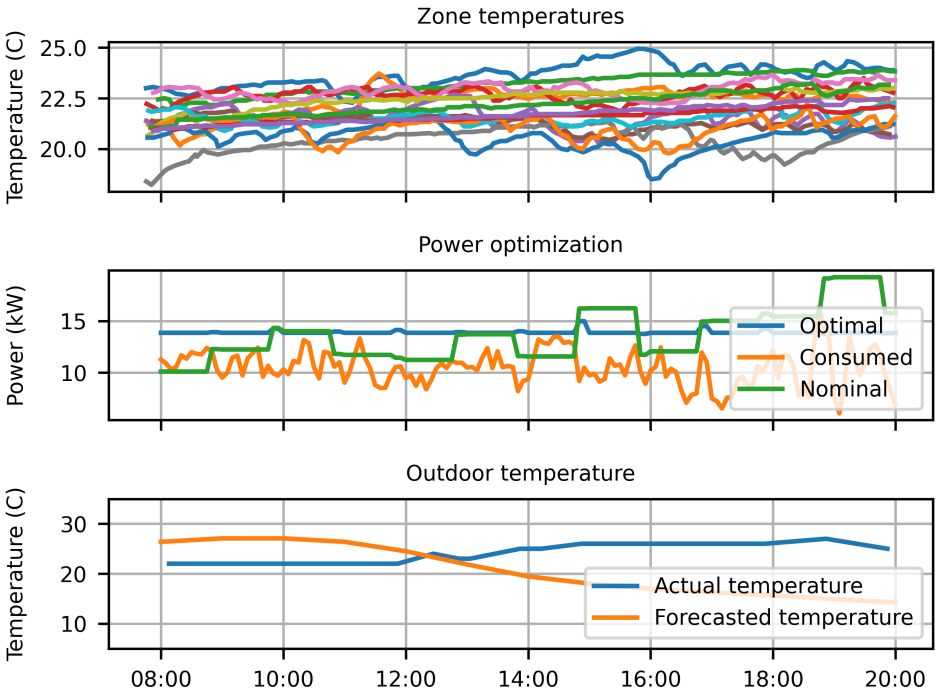

Figure 38. Field testing results for June 22, 2021.

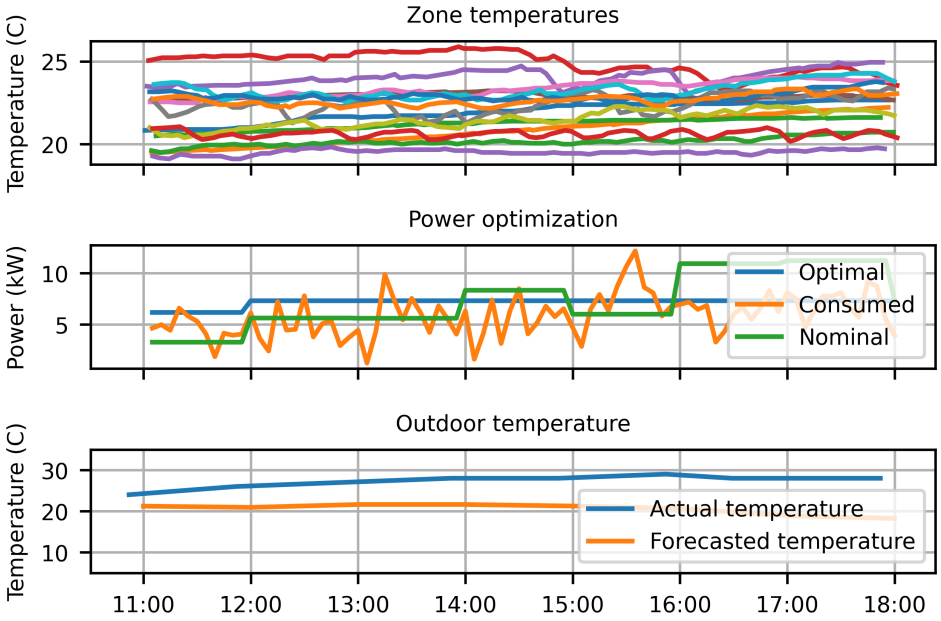

Figure 39. Field testing results for June 23, 2021.

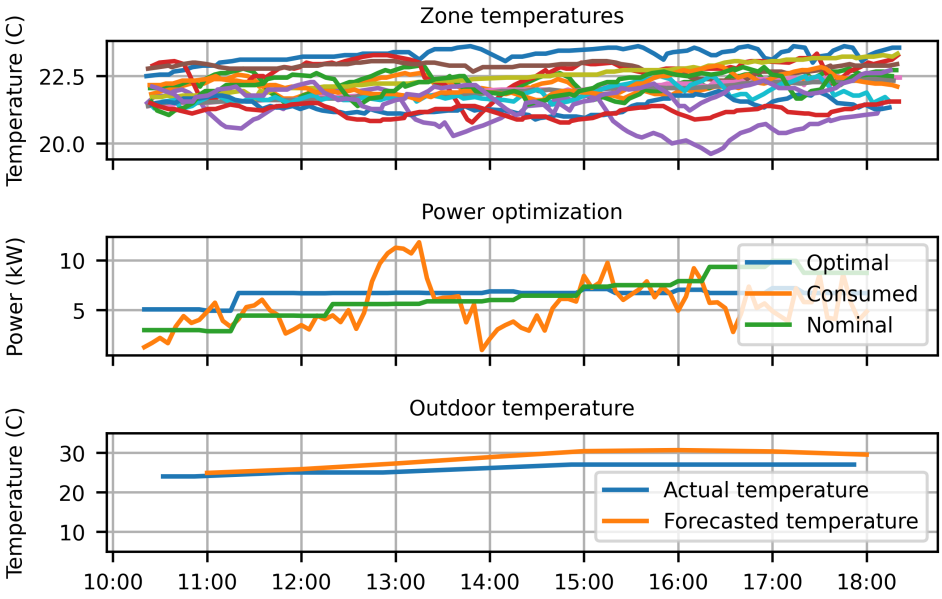

Figure 40. Field testing results for June 24, 2021.

6. SIGNIFICANT ACCOMPLISHMENTS AND CONCLUSIONS

In this project, the team developed and demonstrated: (1) a detailed, simulation-driven understanding of utility-scale demand aggregation and control of load flexibility using model-free control and game theory to harness residential and small-size commercial buildings to provide grid services; (2) an end-to-end simulation-based design of a model-free control framework of building loads that increases customer cost saving (up to ~20%), improves occupants' comfort, reduces peak demand (up to ~30%), and increases utility profit (up to ~20%); and (3) control technology deployment to evaluate the effectiveness and to perform scalability analysis at the utility scale.

7. INVENTIONS, PATENTS, PUBLICATIONS, AND OTHER RESULTS

7.1 PUBLICATIONS

1. K. Amasyali, Y. Chen, and M. Olama, “A Data-Driven, Distributed Game-Theoretic Transactional Control Approach for Hierarchical Demand Response,” IEEE Access, vol. 10, pp. 72279-72289, July 2022.
2. B. Park, Y. Chen, M. Olama, T. Kuruganti, J. Dong, X. Wang, and F. Li, “Optimal Demand Response Incorporating Distribution LMP with PV Generation Uncertainty,” IEEE Transactions on Power Systems, vol. 37, no. 2, pp. 982-995, Mar. 2022.
3. B. Telsang, K. Amasyali, Y. Chen, M. Olama, and S. Djouadi, “Power Allocation by Load Aggregator with Heterogeneous Loads using Weighted Projection,” Energy and Buildings, vol. 244, Article ID 110955, Aug. 2021.
4. X. Kou, F. Li, J. Dong, M. Olama, M. Starke, Y. Chen, and H. Zandi, "A Comprehensive Scheduling Framework using SP-ADMM for Residential Demand Response with Weather and Consumer Uncertainties," IEEE Transactions on Power Systems, vol. 36, no. 4, pp. 3004-3016, July 2021.
5. B. Park and M. Olama, “A Model-Free Voltage Control Approach to Mitigate Motor Stalling and FIDVR for Smart Grids,” IEEE Transactions on Smart Grid, vol. 12, no. 1, pp. 67-78, Jan. 2021.
6. K. Amasyali, Y. Chen, B. Telsang, M. Olama, and S. Djouadi, “Hierarchical Model-free Transactional Control of Building Loads to Support Grid Services,” IEEE Access, vol. 8, pp. 219367-219377, Nov. 2020.
7. X. Kou, Y. Du, F. Li, H. Pulgar-Painemal, H. Zandi, J. Dong, and M. Olama, “Model-Based and Data-Driven HVAC Control Strategies for Residential Demand Response,” IEEE Open Access Journal of Power and Energy, vol. 8, pp. 186-197, May 2021.
8. Y. Chen, B. Park, X. Kou, M. Hu, J. Dong, F. Li, K. Amasyali, and M. Olama, “A Comparison Study on Trading Behavior and Profit Distribution in Local Energy Transaction Games,” Applied Energy, vol. 280, Article ID 115941, Dec. 2020.
9. X. Kou, F. Li, J. Dong, M. Starke, J. Munk, Y. Xue, M. Olama, and H. Zandi, "A Scalable and Distributed Algorithm for Managing Residential Demand Response Programs using Alternating Direction Method of Multipliers (ADMM)," IEEE Transactions on Smart Grid, vol. 11, no. 6, pp. 4871-4882, Nov. 2020.
10. K. Hatipoglu, M. Olama, and Y. Xue, “Model-Free Dynamic Voltage Control of Distributed Energy Resource (DER)-Based Microgrids,” Energies, vol. 13, no. 15, Article ID 3838, July 2020.
11. M. Olama, K. Amasyali, and C. Winstead, “Field Testing of a Hierarchical Model-Free Transactive Control Strategy in a Residential House,” IEEE Energy Conversion Congress and Exposition (ECCE), Oct. 2022.
12. B. Telsang, S. Djouadi, and M. Olama, “Model-Free Building Temperature Control and Power Allocation Under Measurement Time Delays,” Summer Study on Energy Efficiency in Buildings (ACEEE), Aug. 2022.
13. Y. Chen, K. Amasyali, M. Olama, and B. Park, “Robust Solution Approach for Bilevel Demand Response Game at Distribution Level,” IEEE PES General Meeting, July 2022.
14. K. Amasyali, C. Winstead, Y. Chen, J. Munk, M. Olama, and J. Hill, “Hierarchical Model-Free Transactive Control of Residential Building Loads: An Actual Deployment,” IEEE Conference on Innovative Smart Grid Technologies (ISGT), Apr. 2022.

15. B. Park, K. Amasyali, Y. Chen, and M. Olama, "Hierarchical Transactive Control of Flexible Building Loads Under Distribution LMP," IEEE Conference on Innovative Smart Grid Technologies (ISGT), Apr. 2022.
16. Y. Chen and M. Olama, "Collaborative Decision Approach for Electricity Pricing-Demand Response Stackelberg Game," IEEE International Conference on Smart City Innovations, Oct. 2021.
17. S. Morovati, S. M. Djouadi, M. Olama, J. Dong, K. Tomsovic, A. Fathy, and T. Kuruganti "Inertia Emulation Control using Demand Response via 5G Communications," IEEE International Symposium on Power Electronics for Distributed Generation Systems (PEDG), July 2021.
18. K. Amasyali and M. Olama, "Gaussian Process Regression for Aggregate Baseline Load Forecasting," Annual Modeling and Simulation Conference, July 2021.
19. K. Hatipoglu and M. Olama, "A New Distributed Model-Free Control Strategy to Diminish Distribution System Voltage Violations," IEEE PES General Meeting, July 2021.
20. Y. Chen, K. Amasyali, B. Park, M. Olama, B. Telsang, S. M. Djouadi, "Stochastic Pricing Game for Aggregated Demand Response Considering Comfort Level," North American Power Symposium (NAPS), Nov. 2021.
21. T. Wu, M. Olama, and S. Djouadi, "Adaptive Control for Residential HVAC Systems to Support Grid Services," IEEE Conference on Innovative Smart Grid Technologies (ISGT), Feb. 2021.
22. M. Ferrari Maglia, B. Park, and M. Olama, "Design and Evaluation of a Model-Free Frequency Control Strategy in Islanded Microgrids with Power-Hardware-in-the-Loop Testing," IEEE Conference on Innovative Smart Grid Technologies (ISGT), Feb. 2021.
23. Y. Chen, M. Olama, X. Kou, K. Amasyali, J. Dong, and Y. Xue, "Distributed Solution Approach for a Stackelberg Pricing Game of Aggregated Demand Response," IEEE PES General Meeting, Aug. 2020.
24. A. Melin and M. Olama, "A Comfort Model Simplification for Tight Integration with Grid Services Optimizations," IEEE PES General Meeting, Aug. 2020.
25. Y. Chen, X. Kou, M. Olama, H. Zandi, C. Liu, S. Kassaee, B. Smith, A. Abu-Heiba, and A. M. Momen, "Bi-Level Optimization for Electricity Transaction in Smart Community with Modular Pump Hydro Storage," ASME 2020 International Design Engineering Technical Conferences & Computers and Information in Engineering Conference (IDETC/CIE 2020), Aug. 2020.
26. K. Amasyali, Y. Chen, and M. Olama, "Genetic Algorithm for Demand Response: A Stackelberg Game Approach," Spring Simulation Conference (SpringSim'20), May 2020.
27. K. Amasyali, M. Olama, and A. Perumalla, "A Machine Learning-based Approach to Predict the Aggregate Flexibility of HVAC Systems," IEEE Conference on Innovative Smart Grid Technologies (ISGT), Feb. 2020.
28. T. Wu, M. Olama, S.M. Djouadi, J. Dong, Y. Xue, and T. Kuruganti, "Signal Temporal Logic Control for Residential HVAC Systems to Accommodate High Solar PV Penetration," IEEE Conference on Innovative Smart Grid Technologies (ISGT), Feb. 2020.
29. B. Telsang, M. Olama, S. Djouadi, J. Dong, and T. Kuruganti, "Stability Analysis of Model-free Control under Constrained Inputs for Control of Building HVAC Systems," American Control Conference (ACC'19), July 2019.
30. Y. Chen, M. Olama, T. Rajpurohit, J. Dong, and Y. Xue, "Game-Theoretic Approach for Electricity Pricing Between Distribution System Operator and Load Aggregators," IEEE International Conference on Smart Grid and Smart Cities (ICSGSC'19), June 2019.

7.2 INVENTIONS AND COPYRIGHTS

1. M. Olama, K. Amasyali, Y. Chen, S. Djouadi, and T. Kuruganti “Hierarchical Model-Free Transactional Control of Building Loads to Support Grid Services,” ORNL Invention Disclosure 202205211, Oct. 2022.
2. M. Olama, K. Amasyali, Y. Chen, and T. Kuruganti “Hierarchical Model-Free Transactional Control of Building Loads to Support Grid Services,” ORNL Open-Source Software Copyright 81940078, Oct. 2022.

8. PATH FORWARD

The team developed and deployed an open-source, end-to-end software tool for controlling residential and small-size commercial building loads at scale. It enables large-scale residential aggregation to provide a substantial amount of demand-side flexibility to reliably provide grid services. It also facilitates a seamless interface between the grid service requests of utilities and the reliable control required by participating buildings. The project advanced the control formulation from the technology readiness level of this technology from 3 to 7, and it is currently ready for adoption by utilities, building equipment manufacturers, and energy service companies. The team is engaging with utility partners and building equipment manufacturers to demonstrate a seamless transition between the development phase, demonstration phase, and large-scale deployment phase consistent with the long-term objective of the funding agency of using funded research and development programs to promote job creation and economic prosperity within the United States.

9. REFERENCES

[1] S. Huang, Y. Ye, D. Wu, and W. Zuo, "An assessment of power flexibility from commercial building cooling systems in the United States," *Energy,* vol. 221, no. 119571, Apr. 2021.

[2] J. Langevin *et al.*, "US building energy efficiency and flexibility as an electric grid resource," *Joule,* vol. 5, no. 8, pp. 2102–2128, Aug. 2021.

[3] B. Chen, J. Francis, M. Pritoni, S. Kar, and M. Bergés, "Cohort: Coordination of heterogeneous thermostatically controlled loads for demand flexibility," in *Proc. of the 7th ACM International Conference on Systems for Energy-Efficient Buildings, Cities, and Transportation*, pp. 31–40, 2020.

[4] H. Li, Z. Wang, T. Hong, and M. A. Piette, "Energy flexibility of residential buildings: A systematic review of characterization and quantification methods and applications," *Advances in Applied Energy,* vol. 3, no. 100054, Aug. 2021.

[5] S. Lu, W. Gu, S. Ding, S. Yao, H. Lu, and X. Yuan, "Data-driven aggregate thermal dynamic model for buildings: A regression approach," *IEEE Transactions on Smart Grid,* vol. 13, no. 1, pp. 227–242, 2022.

[6] Z. Wang, B. Chen, H. Li, and T. Hong, "AlphaBuilding ResCommunity: A multi-agent virtual testbed for community-level load coordination," *Advances in Applied Energy,* vol. 4, no. 100061, 2021.

[7] A. Roth and J. Reyna, "Grid-interactive efficient buildings technical report series: Whole-building controls, sensors, modeling, and analytics," United States, 2019. [Online]. Available at: https://www.energy.gov/eere/buildings/downloads/grid-interactive-efficient-buildings-technical-report-series-whole-building.

[8] M. Javadi *et al.*, "Optimal operation of home energy management systems in the presence of the inverter-based heating, ventilation and air conditioning system," in *Proc. of the 2020 IEEE International Conference on Environment and Electrical Engineering and the 2020 IEEE Industrial and Commercial Power Systems Europe (EEEIC / I&CPS Europe)*, pp. 1–6, June 2020.

[9] Wang *et al.*, "Stackelberg game-based energy management for a microgrid with commercial buildings considering correlated weather uncertainties," *IET Generation, Transmission & Distribution,* vol. 13, no. 11, pp. 2102–2111, 2019.

[10] M. Vahid-Ghavidel, M. S. Javadi, S. F. Santos, M. Gough, M. Shafie-khah, and J. P. S. Catalão, "Optimal stochastic conditional value at risk-based management of a demand response aggregator considering load uncertainty," in *Proc. of the 2021 IEEE International Conference on Environment and Electrical Engineering and the 2021 IEEE Industrial and Commercial Power Systems Europe (EEEIC / I&CPS Europe)*, pp. 1–6, Sep. 2021.

[11] R. Sharifi, S. H. Fathi, and V. Vahidinasab, "A review on demand-side tools in electricity market," *Renewable and Sustainable Energy Reviews,* vol. 72, pp. 565–572, May 2017.

[12] B. P. Esther and K. S. Kumar, "A survey on residential demand side management architecture, approaches, optimization models and methods," *Renewable and Sustainable Energy Reviews,* vol. 59, pp. 342–351, June 2016.

[13] H. Hao, C. D. Corbin, K. Kalsi, and R. G. Pratt, "Transactive control of commercial buildings for demand response," *IEEE Transactions on Power Systems,* vol. 32, no. 1, pp. 774–783, 2017.

[14] S. Huang, J. Lian, H. Hao, and S. Katipamula, "Transactive control design for commercial buildings to provide demand response," *IFAC-PapersOnLine,* vol. 51, no. 34, pp. 151–156, Jan. 2019.

[15] S. Li, J. Lian, A. J. Conejo, and W. Zhang, "Transactive energy systems: The market-based coordination of distributed energy resources," *IEEE Control Systems Magazine,* vol. 40, no. 4, pp. 26–52, 2020.

[16] M. Yu and S. H. Hong, "A real-time demand-response algorithm for smart grids: A Stackelberg game approach," *IEEE Transactions on Smart Grid,* vol. 7, no. 2, pp. 879–888, 2016.

[17] A. D. Paola, V. Trovato, D. Angeli, and G. Strbac, "A mean field game approach for distributed control of thermostatic loads acting in simultaneous energy-frequency response markets," *IEEE Transactions on Smart Grid,* vol. 10, no. 6, pp. 5987–5999, 2019.

[18] S. Fan, Q. Ai, and L. Piao, "Bargaining-based cooperative energy trading for distribution company and demand response," *Applied Energy,* vol. 226, pp. 469–482, Sep. 2018.
[19] A. Paudel, K. Chaudhari, C. Long, and H. B. Gooi, "Peer-to-peer energy trading in a prosumer-based community microgrid: A game-theoretic model," *IEEE Transactions on Industrial Electronics,* vol. 66, no. 8, pp. 6087–6097, 2019.
[20] M. Marzband, M. H. Fouladfar, M. F. Akorede, G. Lightbody, and E. Pouresmaeil, "Framework for smart transactive energy in home-microgrids considering coalition formation and demand side management," *Sustainable Cities and Society,* vol. 40, pp. 136–154, July 2018.
[21] M. Marzband, F. Azarinejadian, M. Savaghebi, E. Pouresmaeil, J. M. Guerrero, and G. Lightbody, "Smart transactive energy framework in grid-connected multiple home microgrids under independent and coalition operations," *Renewable Energy,* vol. 126, pp. 95–106, Oct. 2018.
[22] C. D. Korkas, S. Baldi, I. Michailidis, and E. B. Kosmatopoulos, "Occupancy-based demand response and thermal comfort optimization in microgrids with renewable energy sources and energy storage," *Applied Energy,* vol. 163, pp. 93–104, Feb. 2016.
[23] A. Kathirgamanathan, M. De Rosa, E. Mangina, and D. P. Finn, "Data-driven predictive control for unlocking building energy flexibility: A review," *Renewable and Sustainable Energy Reviews,* vol. 135, p. 110120, Jan. 2021.
[24] F. Ruelens, B. J. Claessens, S. Vandael, B. D. Schutter, R. Babuška, and R. Belmans, "Residential demand response of thermostatically controlled loads using batch reinforcement learning," *IEEE Transactions on Smart Grid,* vol. 8, no. 5, pp. 2149–2159, 2017.
[25] C. D. Korkas, S. Baldi, and E. B. Kosmatopoulos, "9 - Grid-connected microgrids: Demand management via distributed control and human-in-the-loop optimization," in *Advances in Renewable Energies and Power Technologies*, I. Yahyaoui Ed.: Elsevier, pp. 315–344, 2018.
[26] S. Brandi, M. S. Piscitelli, M. Martellacci, and A. Capozzoli, "Deep reinforcement learning to optimise indoor temperature control and heating energy consumption in buildings," *Energy and Buildings,* vol. 224, p. 110225, Oct. 2020.
[27] Y. Ye, D. Qiu, M. Sun, D. Papadaskalopoulos, and G. Strbac, "Deep reinforcement learning for strategic bidding in electricity markets," *IEEE Transactions on Smart Grid,* vol. 11, no. 2, pp. 1343–1355, 2020.
[28] G. Sivanantham and S. Gopalakrishnan, "A Stackelberg game theoretical approach for demand response in smart grid," *Personal and Ubiquitous Computing,* vol. 24, no. 4, pp. 511–518, Aug. 2020.
[29] C. Shao, Y. Ding, P. Siano, and Z. Lin, "A framework for incorporating demand response of smart buildings into the integrated heat and electricity energy system," *IEEE Transactions on Industrial Electronics,* vol. 66, no. 2, pp. 1465–1475, 2019.
[30] D. Wang *et al.*, "Integrated demand response in district electricity-heating network considering double auction retail energy market based on demand-side energy stations," *Applied Energy,* vol. 248, pp. 656–678, Aug. 2019.
[31] K. Alshehri, J. Liu, X. Chen, and T. Başar, "A game-theoretic framework for multiperiod-multicompany demand response management in the smart grid," *IEEE Transactions on Control Systems Technology,* vol. 29, no. 3, pp. 1019–1034, 2021.
[32] M. Hu, F. Xiao, and S. Wang, "Neighborhood-level coordination and negotiation techniques for managing demand-side flexibility in residential microgrids," *Renewable and Sustainable Energy Reviews,* vol. 135, no. 110248, Jan. 2021.
[33] L. Zheng, B. Zhou, Y. Cao, S. Wing Or, Y. Li, and K. Wing Chan, "Hierarchical distributed multi-energy demand response for coordinated operation of building clusters," *Applied Energy,* vol. 308, no. 118362, Feb. 2022.
[34] C. Lee, L. Park, and S. Cho, "Light-weight Stackelberg game theoretic demand response scheme for massive smart manufacturing systems," *IEEE Access,* vol. 6, pp. 23316–23324, 2018.
[35] R. Zhang, T. Jiang, G. Li, X. Li, and H. Chen, "Stochastic optimal energy management and pricing for load serving entity with aggregated TCLs of smart buildings: A Stackelberg game approach," *IEEE Transactions on Industrial Informatics,* vol. 17, no. 3, pp. 1821–1830, 2021.

[36] H. Wang and S. Wang, "A hierarchical optimal control strategy for continuous demand response of building HVAC systems to provide frequency regulation service to smart power grids," *Energy,* vol. 230, p. 120741, Sep. 2021.
[37] L. Jia and L. Tong, "Dynamic pricing and distributed energy management for demand response," *IEEE Transactions on Smart Grid,* vol. 7, no. 2, pp. 1128–1136, 2016.
[38] K. Amasyali, Y. Chen, B. Telsang, M. Olama, and S. M. Djouadi, "Hierarchical model-free transactional control of building loads to support grid services," *IEEE Access,* vol. 8, pp. 219367–219377, 2020.
[39] B. Telsang, K. Amasyali, Y. Chen, M. Olama, and S. Djouadi, "Power allocation by load aggregator with heterogeneous loads using weighted projection," *Energy and Buildings,* vol. 244, no. 110955, Aug. 2021.
[40] V. C. Pandey, N. Gupta, K. R. Niazi, A. Swarnkar, and R. A. Thokar, "A hierarchical price-based demand response framework in distribution network," *IEEE Transactions on Smart Grid,* vol. 13, no. 2, pp. 1151–1164, Mar. 2022.
[41] M. Yu and S. H. Hong, "Supply–demand balancing for power management in smart grid: A Stackelberg game approach," *Applied Energy,* vol. 164, pp. 702–710, Feb. 2016.
[42] N. Aguiar, A. Dubey, and V. Gupta, "Network-constrained Stackelberg game for pricing demand flexibility in power distribution systems," *IEEE Transactions on Smart Grid,* vol. 12, no. 5, pp. 4049–4058, 2021.
[43] M. Fliess and C. Join, "Model-free control," *International Journal of Control,* vol. 86, no. 12, pp. 2228–2252, Dec. 2013.
[44] F. Lafont, J.-F. Balmat, N. Pessel, and M. Fliess, "A model-free control strategy for an experimental greenhouse with an application to fault accommodation," *Computers and Electronics in Agriculture,* vol. 110, pp. 139–149, Jan. 2015.
[45] C. Join, F. Chaxel, and M. Fliess, "“Intelligent” controllers on cheap and small programmable devices," in *Proc. of the 2013 Conference on Control and Fault-Tolerant Systems (SysTol)*, pp. 554–559, Oct. 2013.
[46] H. Hao, B. M. Sanandaji, K. Poolla, and T. L. Vincent, "Aggregate flexibility of thermostatically controlled loads," *IEEE Transactions on Power Systems*, vol. 30, no. 1, pp. 189–198, Jan. 2015.
[47] P. Wang, D. Wu, and K. Kalsi, "Flexibility estimation and control of thermostatically controlled loads with lock time for regulation service," *IEEE Transactions on Smart Grid,* vol. 11, no. 4, pp. 3221–3230, 2020.
[48] R. Gondhalekar, F. Oldewurtel, and C. N. Jones, "Least-restrictive robust periodic model predictive control applied to room temperature regulation," *Automatica,* vol. 49, no. 9, pp. 2760–2766, Sep. 2013.
[49] P. Boudreaux, J. Munk, R. Jackson, A. Gehl, A. Parkison, and J. Nutaro, "Improving heat pump water heater efficiency by avoiding electric resistance heater use," Technical Report, Oak Ridge National Laboratory, ORNL/TM-2014/483, 2014.
[50] S. Bandyopadhyay, T. Ganu, H. Khadilkar, and V. Arya, "Individual and aggregate electrical load forecasting: One for all and all for one," in *Proc. of the 2015 ACM 6th International Conference on Future Energy Systems*, pp. 121–130, 2015.
[51] Z. M. Fadlullah, D. M. Quan, N. Kato, and I. Stojmenovic, "GTES: An optimized game-theoretic demand-side management scheme for smart grid," *IEEE Systems Journal,* vol. 8, no. 2, pp. 588–597, 2014.
[52] P. Yang, G. Tang, and A. Nehorai, "A game-theoretic approach for optimal time-of-use electricity pricing," *IEEE Transactions on Power Systems,* vol. 28, no. 2, pp. 884–892, May 2013.
[53] Y. Chen, M. Olama, T. Rajpurohit, J. Dong, and Y. Xue, "Game-theoretic approach for electricity pricing between distribution system operator and load aggregators," in *Proc. of the 3rd International Conference on Smart Grid and Smart Cities (ICSGSC)*, pp. 176–181, June 2019.
[54] Y. Chen, M. Olama, X. Kou, K. Amasyali, J. Dong, and Y. Xue, "Distributed solution approach for a Stackelberg pricing game of aggregated demand response," in *Proc. of the IEEE PES General Meeting*, Aug. 2020.

[55] Y. Chen and M. Olama, "Collaborative decision approach for electricity pricing-demand response Stackelberg game," in *Proc. of the 5th IEEE International Conference on Smart City Innovations*, Oct. 2021.
[56] M. Fliess and C. Join, "Model-free control and intelligent PID controllers: Towards a possible trivialization of nonlinear control," *IFAC Proc. Volumes,* vol. 42, no. 10, pp. 1531–1550, Jan. 2009.
[57] P.-A. Gédouin, E. Delaleau, J.-M. Bourgeot, C. Join, S. Arbab Chirani, and S. Calloch, "Experimental comparison of classical PID and model-free control: Position control of a shape memory alloy active spring," *Control Engineering Practice,* vol. 19, no. 5, pp. 433–441, May 2011.
[58] V. Milanes, J. Villagra, J. Perez, and C. Gonzalez, "Low-speed longitudinal controllers for mass-produced cars: A comparative study," *IEEE Transactions on Industrial Electronics,* vol. 59, no. 1, pp. 620–628, Jan. 2012.
[59] E. Delaleau, "A proof of stability of model-free control," in *Proc. of the IEEE Conference on Norbert Wiener in the 21st Century (21CW)*, pp. 1–7, June 2014.
[60] DOE. "Building Energy Codes Program." Available at: https://www.energycodes.gov/development.
[61] M. Sengupta, Y. Xie, A. Lopez, A. Habte, G. Maclaurin, and J. Shelby, "The National Solar Radiation Data Base (NSRDB)," *Renewable and Sustainable Energy Reviews,* vol. 89, pp. 51–60, June 2018.
[62] J. Dong, J. Munk, B. Cui, P. R. Boudreaus, and T. Kuruganti, "Machine-learning model of electric water heater for electricity consumption prediction," in *International High Performance Buildings Conference*, 2018.
[63] J. Dong *et al.*, "Model predictive control of building on/off HVAC systems to compensate fluctuations in solar power generation," in *Proc. of the 9th IEEE International Symposium on Power Electronics for Distributed Generation Systems (PEDG)*, pp. 1–5, June 2018.
[64] L. Wu, M. Shahidehpour, and T. Li, "Stochastic security-constrained unit commitment," *IEEE Transactions on Power Systems*, vol. 22, no. 2, pp. 800–811, May 2007.
[65] Y. Chen and M. Hu, "Swarm intelligence-based distributed stochastic model predictive control for transactive operation of networked building clusters," *Energy and Buildings*, vol. 198, pp. 207–215, Sep. 2019.
[66] M. Kazemi, H. Zareipour, M. Ehsan, and W. D. Rosehart, "A robust linear approach for offering strategy of a hybrid electric energy company," *IEEE Trans. Power Syst.*, vol. 32, no. 3, pp. 1949–1959, 2017.
[67] Y. Chen *et al.*, "Bi-level optimization for electricity transaction in smart community with modular Pump hydro storage," in *Proc. of the ASME 2020 International Design Engineering Technical Conferences and Computers and Information in Engineering Conference*, 2020, p. V006T06A016.
[68] Y. Chen *et al.*, "A comparison study on trading behavior and profit distribution in local energy transaction games," *Appl. Energy*, vol. 280, p. 115941, 2020.
[69] M. Kazemi, H. Zareipour, N. Amjady, W. D. Rosehart, and M. Ehsan, "Operation scheduling of battery storage systems in joint energy and ancillary services markets," *IEEE Trans. Sustain. Energy*, vol. 8, no. 4, pp. 1726–1735, 2017.
[70] Y. Chen and M. Hu, "Balancing collective and individual interests in transactive energy management of interconnected micro-grid clusters," *Energy*, vol. 109, pp. 1075–1085, 2016.
[71] OpenWeather API. https://openweathermap.org/api.
[72] VOLTTRON. https://volttron.org/.
[73] Ace IoT. https://aceiotsolutions.com/.
[74] A. Wächter and L. T. Biegler, "On the implementation of an interior-point filter line-search algorithm for large-scale nonlinear programming," *Mathematical Programming,* vol. 106, no. 1, pp. 25–57, Mar. 2006.
[75] Influxdata. https://www.influxdata.com/.
[76] Docker. https://www.docker.com/.
[77] Grafana. https://grafana.com/.